ABSTRACT

HIDEHIRO SEGAWA. Optimum Flap Angles for Roll Control on Wings with Multiple Trailing-Edge Flaps. (Under the direction of Dr. Ashok Gopalarathnam.)

This research effort explores the use of multiple trailing-edge flaps for efficiently generating rolling moment on aircraft. Using the concept of basic and additional lift distributions, the induced drag of the wing is expressed in terms of the flap angles. The theory of relative extrema is then used to determine the optimum flaps angles for minimum induced drag with a constraint on the rolling moment. By setting the mean of the flap angle for operation of the wing within the low-drag range, profile drag is also minimized. The general methodology can also be used on tailless aircraft and to study the effect of failure modes such as a stuck flap. The results show that multiple flaps can be used to generate rolling moments with lower drag than when ailerons are used. They also provide redundancy that helps efficiently handle control failures such as stuck flaps. The current research serves as a starting point for further investigation into the use of multiple flaps for efficient aircraft control.

Optimum Flap Angles for Roll Control on Wings with Multiple Trailing-Edge Flaps

by

Hidehiro Segawa

A thesis submitted to the Graduate Faculty of
North Carolina State University
in partial fulfillment of the
requirements for the Degree of
Master of Science

Aerospace Engineering

Raleigh, NC
2007

APPROVED BY:

Dr. Ashok Gopalarathnam
Advisory Committee Chairman

Dr. Charles E. Hall, Jr.
Advisory Committee Member

Dr. Agnes Szanto
Advisory Committee Member

BIOGRAPHY

Hidehiro Segawa was born to Yorihide and Umeyo Segawa May 27th, 1981 in Hitachi, Japan. The youngest of three children, Hidehiro lived until his graduation from Mito-Sakuranomaki High School in the Spring of 2000.

In July of 2000 he moved to the United States for study. He spent two years at Thiel College in Pennsylvania to study Physics. In the summer of 2002 Hidehiro transferred to North Carolina State University to major in Aerospace Engineering, which had been his interest since his childhood. Three years later he graduated from the university with a Bachelor of Science in Aerospace Engineering.

In the Fall of 2005 Hidehiro decided to remain at the university and enroll as a Master's student in Aerospace Engineering. He joined the Applied Aerodynamics group at NC State in the Spring of 2006 under the advisement of Dr. Ashok Gopalarathnam, who supported his Master's work.

After completion of his Master's degree Hidehiro plans to remain at NC State to pursue a doctoral degree in Aerospace Engineering focusing on airfoil and wing aerodynamics under the advisement of Dr. Ashok Gopalarathnam.

ACKNOWLEDGEMENTS

I would like to express my appreciation to Dr. Ashok Gopalarathnam for his guidance in my thesis research. To study Applied Aerodynamics under him was my dream since I came to the department of Mechanical and Aerospace Engineering at NC State University. I am really grateful that he gave me a chance to accomplish this goal.

I would like to express my appreciation to KalScott Engineering for their financial support. I also would like to thank Dr. Charles E. Hall, Jr. for being my thesis committee member. He is one of the most influential professors in the Aerospace Engineering program, and I appreciate his support. I also would like to acknowledge Dr. Agnes Szanto from Mathematics department for her kindness and for being a committee member.

Additionally, I would like to thank my fellow colleagues, Gregory Z McGowan, Aaron Anthony Cusher, Craig Allen Cox, Stearns Nicholas Heinzen, Blaine A Levedahl and others for their support, additional assistance and friendship.

Lastly, I really appreciate my family for all their support and prayers for my success. Completing a degree in a foreign country was very challenging for me, but because of their understanding and support, it came true. Especially, I would like to thank my father who passed away over ten years ago. His hard work made it possible for me to study in a foreign country, and his research interest in fluid dynamics motivated me to study Aerospace Engineering. I know that he is still in my heart and very pleased with the completion of my Master's work. Finally, I would like to thank my mother and sisters for their prayers. I cannot express how grateful I am that they support my achievement. Thank you all.

Table of Contents

List of Tables

List of Figures

Nomenclature

A_1, A_2, A_n coefficients of Fourier series

ac aerodynamic center

AR wing aspect ratio

b wingspan

$\bar{c}$ mean aerodynamic chord

C_{D_i} aircraft total induced drag coefficient

CG center of gravity

C_L aircraft lift coefficient

C_l airfoil lift coefficient

C_{L_0} aircraft lift coefficient for zero α

C_{la} additional lift coefficient

$C_{la,1}$ additional lift coefficient defined at C_L of one

C_{lb} basic lift coefficient

$C_{lb,camber}$ basic lift coefficient due to airfoil camber

$C_{lb,flap}$ basic lift coefficient due to flap deflection

$C_{lb,twist}$ basic lift coefficient due to wing twist

C_{m_0} zero-lift airfoil pitching moment

$C_{m_{ac}}$ airfoil pitching moment coefficient about the aerodynamic center

$\left(C_{M_{ac_w}}\right)_{basic}$ aircraft pitching moment coefficient about the aerodynamic center resulting from the basic lift distribution

$C_{M,cg}$ aircraft pitching moment coefficient about the center of gravity

$\left(C_{M_{ac_w}}\right)_{sections}$ aircraft pitching moment coefficient about the aerodynamic center resulting from the airfoil sections

C_R aircraft rolling moment coefficient

$c(y)$ spanwise chord distribution

dL elemental loading

H objective function

LDR low drag range

LHS left hand side

NLF natural laminar flow

N number of flaps over the span of wing

NP neutral point

Re Reynolds number

RHS right hand side

S wing area

SM static margin

TAT thin airfoil theory

TE trailing edge

V_∞ freestream velocity

W aircraft weight

w normalwash/downwash in the Trefftz-plane

X_{ac} longitudinal location of the aerodynamic center

X_{cg} longitudinal location of the center of gravity

α angle of attack

δ_f flap angle

$\bar{\delta}_f$ mean flap angle

$\hat{\delta}_f$ variation flap angle about the mean

Γ bound vorticity strength

λ Lagrange multiplier

$\Lambda_{c/4}$ quarter-chord sweep angle

θ_f angular location of flap hinge in radians

Subscripts

$desired$ desired condition

f flap

$ideal$ ideal condition

∞ freestream condition

ref reference

$wing$ wing

Chapter 1

Introduction

Over the hundred years of aviation history, aircraft performance has improved dramatically as a result of better understanding of various design issues. These improvements include airfoil and wing designs, engine performance, flight control technology, utility of new materials, and so on. This study focuses on one aspect of improving airfoil and wing aerodynamics, which is an avenue to achieving better aircraft performance.

1.1 Background

Traditionally, trailing-edge flaps (TE flaps) are used to achieve higher lift for take-off and landing. In certain applications, however, they are also used for achieving lower drag. The use of TE flaps for low drag is popular in high-performance sailplanes. Known as cruise flaps, these devices enable achievement of low drag over a wide range of flight speeds. Conceived first by Pfenninger[3,4] in 1947, a cruise flap, when used on a natural laminar flow (NLF) airfoil,[5–10] enables adjustment of the C_l range of the drag bucket so that laminar flow and the accompanying low drag can be achieved at off-design C_l values. Since then, many NLF airfoils have been designed to use cruise flaps.[11] The use of multiple TE flaps along the wing span has also been proposed by several researchers[12,13] for drag reduction

and wing-weight reduction.

Research projects in the NCSU Applied Aerodynamics Group has recently focused on the use of TE flaps on aircraft wings. These projects have resulted in (i) automation of single and multiple TE flaps based on surface pressure measurements,[14,15] (ii) semi-analytical approaches to the determination of ideal flap angles on a wing with multiple TE flaps,[16] (iii) and the use of multiple TE flaps to achieve low drag on tailless aircraft while satisfying the necessary pitching moment constraints.[17] The results from these studies show that multiple TE flaps are an efficient way to adapt a wing for different flight conditions. The current effort builds on these past projects to explore the use of multiple TE flaps in efficiently generating rolling moment on an adaptive wing.

The original idea of the adaptive wing came from the bird and insect flights. These creatures are able to adjust not only the wing aspect ratio and wing loading but also the spanwise twist on the wing to achieve optimal lift distribution. Fig 1.1 is a sketch drawn by Otto Lilienthal, which shows how the spanwise twist is distributed on a wing for bird flight.

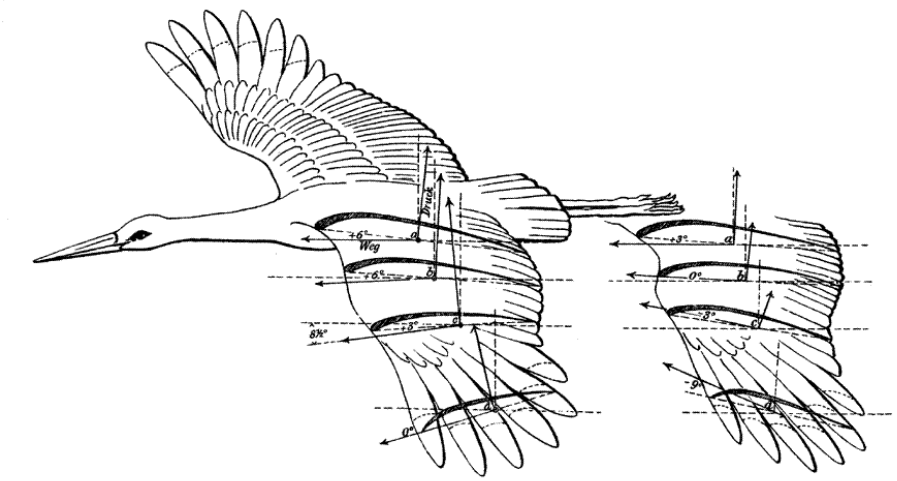

Figure 1.1: Adaptive wing of bird flight.[1]

Theoretically, tuning the spanwise twist on a wing is the most accurate way of generating the optimal lift distribution because each section of the wing can deflect for desirable twist angle. However, it is still difficult for engineers to create such a twistable wing mainly due to structural reasons. Instead, it is possible to manufacture a wing with the multiple TE flaps which serves nearly the same function as the twistable wing. A simple sketch of a wing with the multiple TE flaps is shown in the Fig 1.2. These TE flaps are controllable individually just like a bird adjusts the spanwise twist on the wing to generate the ideal distribution.

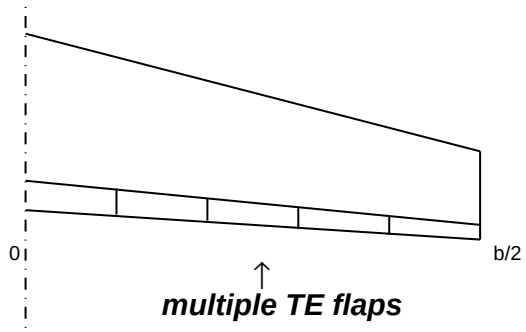

Figure 1.2: Schematic representation of the multiple trailing-edge flaps (right side shown).

The adaptive wing can be used not only for producing the optimum lift distribution, but also for aircraft control. Azuma[18] studied the flight dynamics of flying creatures and described the control with the use of adaptive wing. They trim the body not by having horizontal and vertical tails, but adjusting the spanwise twist on the wing. Recent research[17] proved that this was possible with the multiple TE flaps if they were placed on a swept flying wing. However, this research was only for a longitudinal control. The current research work explores the use of multiple TE flaps for roll control. Traditionally, the rolling moment is generated by ailerons. The current work explores if multiple TE flaps can generate moment

with reduced induced drag. The current work is a first step in exploring the use of distributed controls (TE flaps) for aircraft control.

In addition, the current work also explores the use of TE flaps for generating rolling moment on a tailless aircraft, where the TE flaps have to also satisfy a pitching moment constraint. With continued interest in tailless aircraft such as the Blended-wing body (BWB) concept (Fig 1.3), it is worthwhile to explore the efficient use of distributed controls on such configurations. Finally, one of the benefits of using distributed controls is in the redundancy they provide in case of failure of one or more components. Towards understanding this capability, the current study also explores the efficient use of the distributed controls in the event of a failure of one of the TE flaps.

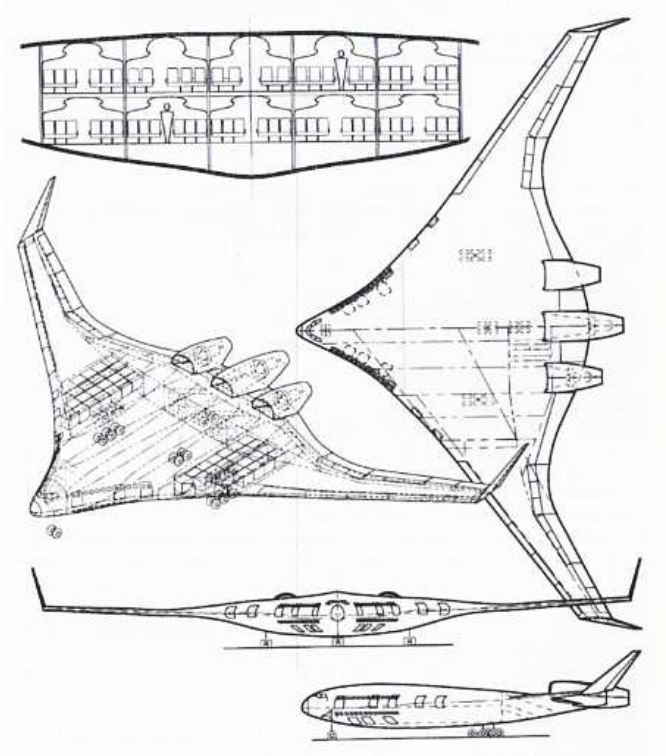

Figure 1.3: Blended-wing-body (BWB) airplane concept.[2]

1.2 Outline of Thesis

This chapter has described a brief history of how the current research topic has evolved from the previous studies. Also the motivation for conducting the current research with the multiple TE flaps has been presented.

Moving forward, Chapter 2 describes the background information and methodology utilized in this research. First presented is the background information relating to achievement of minimum induced and profile drag, as well as the concept of additional and basic lift distributions and their superposition. Next section is a derivation of the rolling moment equation for the multiple TE flaps, followed by a brief description of the pitching moment constraint.

In the procedure section, minimization of induced drag without constraints is first described. Then a single constraint of the rolling moment is described. In the following section, the double constraints of the roll and pitch is presented. Finally, for a case of the stuck flap, the equation is solved for the deflection angles of the controllable flaps.

Results using the methodology are presented in Chapter 3 for several example geometries. The first case is the single constraint of rolling moment. The lift distributions are obtained for two types of wing and airfoil for different values of the desired rolling moment. Then the results are shown for the double constraints of roll and pitch for swept wings. Lastly, the lift distributions for the stuck flap case on a straight wing are presented and discussed.

Chapter 4 presents brief conclusion of the research as well as some suggested follow-on research.

Chapter 2

Methodology

2.1 Background

In this section, background information is presented on well-known elements of applied mathematics and aerodynamics that are used in the development of the current method. Subsection 2.1.1 describes the theory of the relative extrema of multi-variable functions with and without constraints. Subsection 2.1.2 describes the derivation of the optimum flap angles for the rolling moment. Subsection 2.1.3 presents a brief review of the concept of basic and additional lift distributions. Subsection 2.1.4 presents the induced drag of superposed lift distributions based on Munk's theorems. Lastly, Subsection 2.1.5 reviews the formulation of pitching moment due to the multiple TE flaps.

2.1.1 Relative Extrema of Multi-Variable Functions with and without Constraints

This subsection presents a mathematical technique for solving the minimum value of a multi-variable function with and without constraints, which is discussed in more detail in textbooks such as by Bryson and Ho.[19] Consider a function, $f(x_i)$, of several variables x_i. The necessary condition for an extremum is that the first

derivative of the function with respect to every variable be zero, as follows:

$$\frac{\partial f}{\partial x_i} = 0 \tag{2.1}$$

In addition, the sufficient condition for a minimum of f is that the Hessian matrix, formed by elements $\frac{\partial^2 f}{\partial x_i \partial x_j}$ be positive definite.

For a case with equality constraints given by $g_j(x_i) = 0$, the problem is solved by modifying the objective function using unknown Lagrange multipliers, λ_j, as follows:

$$H = f(x_i) + \sum_{j=1}^{K} \lambda_j g_j(x_i) \tag{2.2}$$

The relative extremum is found by setting the partial derivatives of H with respect to x_i and λ_j to be zero, as follows

$$\frac{\partial H}{\partial x_i} = 0 \tag{2.3}$$

$$\frac{\partial H}{\partial \lambda_j} = 0 \tag{2.4}$$

2.1.2 Rolling Moment and Optimum Lift Distribution

The rolling moment is generated due to a different amount of total lift force produced between right and left sides of the wing. To analyze this moment explicitly, first of all, the total lift force is derived using an element of the loading, dL. Then the rolling moment due to the element of lift is calculated. This is shown in Fig 2.1.

According to the definition in this figure, the rolling moment due to dL is expressed as shown in Eqn 2.5.

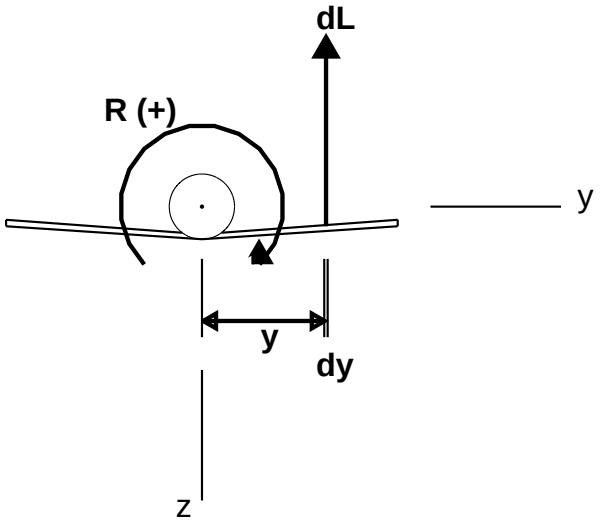

Figure 2.1: Rolling moment due to dL (rear view).

$$dR = (-dL) \cdot y \tag{2.5}$$

The total rolling moment of an aircraft is obtained by integrating this element of rolling moment for a whole span.

$$R = -\int_{-\frac{b}{2}}^{\frac{b}{2}} \left(\frac{1}{2}\rho V_\infty^2\right) cC_l y dy \tag{2.6}$$

It is then non-dimensionalized and re-written as Eqn 2.7.

$$C_R = -\frac{1}{S_{ref} b_{ref}} \int_{-\frac{b}{2}}^{\frac{b}{2}} cC_l y dy = -\frac{2}{S_{ref} b_{ref}} \int_{-\frac{b}{2}}^{\frac{b}{2}} \frac{\Gamma}{V_\infty} y dy \tag{2.7}$$

This is the equation of the rolling moment coefficient, which is calculated from the spanwise lift distribution. The equation is reformed further more to apply for the multiple TE flaps in the Sec. 2.2.

In the remainder of this subsection, the theoretical optimum for spanwise lift distribution for minimum induced drag with and without a rolling moment

constraint is presented. For this derivation of the optimum lift distribution, the standard solution procedure for lifting line theory is used. As described in several textbooks such as Anderson,[20] a coordinate transformation from y to θ is used:

$$y = -\frac{b}{2}\cos\theta \tag{2.8}$$

The spanwise distribution of bound circulation, $\Gamma(y)$, is expressed in as a Fourier series in θ as using N terms as:

$$\Gamma(\theta) = 2bV_\infty \sum_{n=1}^{N} A_n \sin(n\theta) \tag{2.9}$$

For this representation, it can be shown that the lift coefficient C_L, the induced drag coefficient C_{D_i} and rolling moment coefficient C_R can be written in terms of the Fourier coefficients as:

$$C_L = A_1 \pi \frac{b^2}{S} \tag{2.10}$$

$$C_{D_i} = \pi(AR)A_1^2\left[1 + \sum_{2}^{N} n\left(\frac{A_n}{A_1}\right)^2\right] \tag{2.11}$$

$$C_R = A_2 \frac{\pi b^2}{4S} \tag{2.12}$$

It follows, therefore, that for minimum C_{D_i} at a specified C_L, all Fourier terms A_2, A_3, and higher are zero and the optimum lift distribution is

$$\Gamma(\theta) = 2bV_\infty A_1 \sin\theta = 2bV_\infty\left(\frac{C_L S}{\pi b^2}\right)\sin\theta \tag{2.13}$$

which results in the well-known elliptical loading:

$$\Gamma(y) = \Gamma_0 \sqrt{1 - \left(\frac{2y}{b}\right)^2} \tag{2.14}$$

and the corresponding C_{D_i} is

$$C_{D_i} = \frac{{C_L}^2}{\pi AR} \tag{2.15}$$

When the rolling moment coefficient, C_R, is also specified, the solution for minimum C_{D_i} is satisfied by all Fourier terms A_3, A_4 and higher getting set to zero. The resulting lift distribution is

$$\Gamma(\theta) = 2bV_\infty \Big[A_1 \sin\theta + A_2 \sin(2\theta) \Big] = 2bV_\infty \Big[C_L \frac{S}{\pi b^2} \sin\theta + C_R \frac{4S}{\pi b^2} \sin(2\theta) \Big] \tag{2.16}$$

and the corresponding C_{D_i} is

$$C_{D_i} = \frac{1}{\pi AR} \Big[{C_L}^2 + 32 {C_R}^2 \Big] \tag{2.17}$$

2.1.3 Basic and Additional Lift Distributions

As it shown in the previous chapter, several ideas were studied to achieve a desirable lift distribution along the wing span. Some use geometric and aerodynamic twist distributions and flap deflections.

The lift distribution is also affected by angle of attack, spanwise chord distribution (taper), and wing sweep. The net distribution is determined by all of these factors. Therefore, the distribution needs to be decomposed so that it can be analyzed from different aspects. This is why the concept of basic and additional lift distributions, discussed in Kuethe and Chow,[21] is very useful. As per this concept, it is found that the net C_l distribution can be expressed as a superposition of basic

and additional distributions as follows:

$$C_l(y) = C_{lb}(y) + C_{la}(y) \tag{2.18}$$

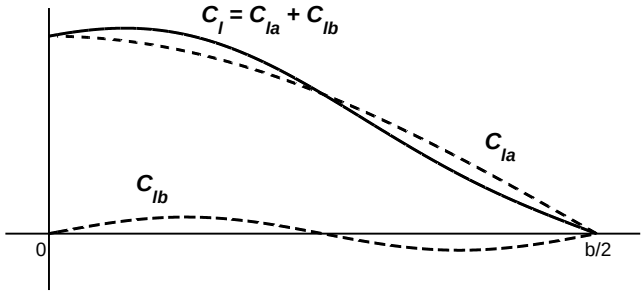

Figure 2.2: Basic and additional lift distributions.

The basic distribution is defined at wing C_L=0, and it is determined by the geometric and aerodynamic twist, the flap deflection, and a change of airfoil or its camber along span.

$$C_{lb} = C_{lb,twist} + C_{lb,camber} + C_{lb,flap} \tag{2.19}$$

The additional distribution, on the other hand, is the distribution when there is no twist or flap deflection on the wing. It is also determined by wing C_L, which is a linear function of angle of attack if attached flow on the wing is assumed. For this case, the wing C_L is set to unity to obtain the $C_{la,1}$, then a desired C_L is substituted to calculate the additional distribution, as follows:

$$C_{la} = C_L C_{la,1} \tag{2.20}$$

It is necessary to mention here that both basic and additional distributions

are affected by the wing planform which are taper and sweep of the wing. The concept of this superposition of these distributions is shown in Fig 2.2.

2.1.4 Induced Drag of Superposed Lift Distribution

It is well-known in wing aerodynamics that induced drag can be calculated through the superposition of the lift distribution. Eqn 2.21 shows how the induced drag is determined for a planar wing from the bound vorticity distribution, $\Gamma(y)$, and the associated Trefftz-plane downwash, $w(y)$.

$$D_{induced} = \frac{\rho}{2} \int_{-\frac{b}{2}}^{\frac{b}{2}} \Gamma(y) w(y) dy \tag{2.21}$$

Using a small angle assumption, the Trefftz-plane induced angle of attack can be written as:

$$\alpha_i(y) = \frac{w}{V_\infty}(y) \tag{2.22}$$

From Kutta-Joukowski theorem, the lift force is expressed with the circulation, which is shown in Eqn 2.23 or non-dimensionalized of Eqn 2.24.

$$L'(y_0) = \rho V_\infty \Gamma(y_0) \tag{2.23}$$

$$\frac{\Gamma}{V_\infty}(y) = \frac{cC_l(y)}{2} \tag{2.24}$$

The induced drag coefficient is expressed and shown as Eqn. 2.25 based on Eqn 2.22 and Eqn 2.24.

$$C_{D_i} = \frac{1}{S} \int_{-\frac{b}{2}}^{\frac{b}{2}} cC_l(y) \alpha_i(y) dy \tag{2.25}$$

The lift coefficient is also derived in the following Eqn 2.26 by the Kutta-Joukowski theorem.

$$C_L = \frac{1}{S}\int_{-\frac{b}{2}}^{\frac{b}{2}} cC_l(y)dy = \frac{2}{V_\infty S}\int_{-\frac{b}{2}}^{\frac{b}{2}} \Gamma(y)dy \tag{2.26}$$

Several theories of the induced drag were derived by Max Munk[22] and one of them states that the induced drag can be determined by adding the contributions from the interaction of the elementary lift distributions and their corresponding downwash distributions. Consider a wing with N TE flaps. Let the total lift distribution be expressed as a superposition of the additional lift and N basic lift distributions corresponding to the N flaps. With this approach, total induced drag for that system can be written in terms of the contributions as follows:

$$D_i = D_{aa} + \sum_{i=1}^{N}(D_{ai} + D_{ia}) + \sum_{j=1}^{N}\sum_{i=1}^{N} D_{ij} \tag{2.27}$$

Munk's mutual drag theorem[23] aids to simplify such expression by saying that the drag induced by element 1 on element 2 is equal to the drag induced by element 2 on element 1. Therefore, $D_{12} = D_{21}$ and so on for all other elements. Also each of these induced drag is non-dimensionalized based on the following equations.

$$\frac{D_{aa}}{q_\infty S} = \frac{{C_L}^2}{2S}\int_{-\frac{b}{2}}^{\frac{b}{2}} cC_{l_a}(y)\alpha_{i_a}(y)dy = {C_L}^2 C_{D_{aa}} \tag{2.28}$$

$$\frac{D_{ai}}{q_\infty S} = \frac{C_L}{2S}\int_{-\frac{b}{2}}^{\frac{b}{2}} cC_{l_a}(y)\alpha_{i_i}(y)dy\delta_i = C_L C_{D_{ai}}\delta_i \tag{2.29}$$

$$\frac{D_{ij}}{q_\infty S} = \frac{1}{2S}\int_{-\frac{b}{2}}^{\frac{b}{2}} cC_{l_i}(y)\alpha_{i_j}(y)dy\delta_i\delta_j = C_{D_{ij}}\delta_i\delta_j \tag{2.30}$$

Finally, the induced drag due to the N multiple TE flaps can be written as Eqn 2.31.

$$
\begin{aligned}
C_{D_i} &= {C_L}^2 C_{D_{aa}} + C_{D_{11}} {\delta_1}^2 + \cdots + C_{D_{NN}} {\delta_N}^2 \\
&+ 2C_L C_{D_{a1}} \delta_1 + \cdots + 2C_L C_{D_{aN}} \delta_N + 2C_{D_{12}} \delta_1 \delta_2 + \cdots + 2C_{D_{1N}} \delta_1 \delta_N \\
&+ 2C_{D_{23}} \delta_2 \delta_3 + \cdots + 2C_{D_{2N}} \delta_2 \delta_N + \cdots + 2C_{D_{(N-1)N}} \delta_{(N-1)} \delta_N
\end{aligned}
\tag{2.31}
$$

2.1.5 Pitching Moment with Multiple TE Flaps

Recent work by Cusher and Gopalarathnam[17] has explored the use multiple TE flaps on tailless aircraft; where the pitching moment about the center of gravity (CG) is constrained to be zero for pitch trim. This section presents some important methods from that research.

Figure 2.3 shows the forces and moments applied to the reference section of the wing. The moment at CG is affected by a moment occurs at the aerodynamic center of a wing (neutral point: NP), and another moment due to an aerodynamic lift force on the wing. This is shown in Eqn 2.32 where $\frac{(X_{ac}-X_{cg})}{\bar{c}}$ is commonly known as the static margin. It is noted that the value of the C_{mac_w} will depend on the wing flap angles.

$$
C_{m_{cg}} = C_{m_{ac_w}} - C_L \frac{(X_{ac} - X_{cg})}{\bar{c}} \tag{2.32}
$$

For the longitudinal trim of an airplane, the moment about the center of gravity (CG) needs to be zero ($C_{m_{cg}} = 0$), so that the equation can be rewritten as follows:

$$
C_{m_{ac_w}} = C_L \frac{(X_{ac} - X_{cg})}{\bar{c}} \tag{2.33}
$$

Therefore, if the static margin and a desired C_L of an aircraft are known, then the required $C_{M_{ac_w}}$ can be calculated by this formula.

A fundamental equation for the pitching moment about the aerodynamic cen-

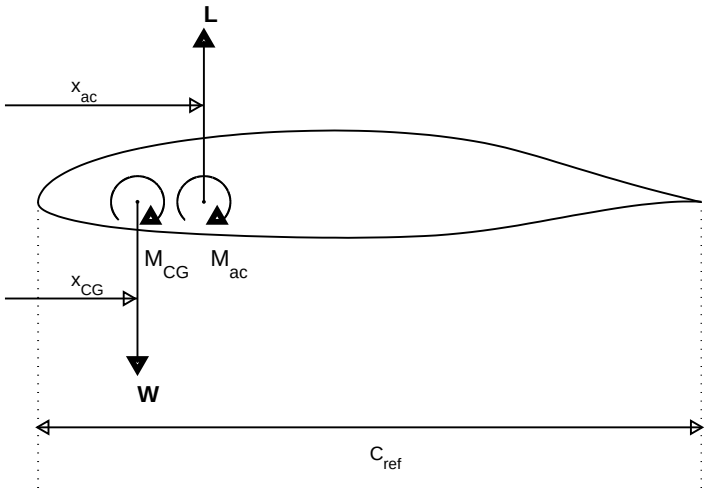

Figure 2.3: Forces applied to the reference section representing the relationship between pitching moments and SM.

ter of an aft-swept wing is shown in Eq. 2.34.

$$C_{M_{ac_w}} = \frac{1}{S\bar{c}} \left\{ \int_{\frac{-b}{2}}^{\frac{b}{2}} C_{m_{ac}}(y) c(y)^2 dy + \int_{\frac{-b}{2}}^{\frac{b}{2}} C_{lb}(y)[X_{ac,wing} - X_{ac}(y)] c(y) dy \right\} \quad (2.34)$$

This equation simply explains that the total pitching moment of a wing at the aerodynamic center is computed by summing two wing spanwise integrals of (1) sectional pitching moment effect and (2) basic lift distribution multiplied by its moment arm based on the wing aerodynamic center. For clarity, part (1) of Eq. 2.34 is referred to as $\left(C_{M_{ac_w}}\right)_{sections}$, and (2) is referred to as $\left(C_{M_{ac_w}}\right)_{basic}$. Then the equation is simply rewritten as indicated by Eq. 2.35.

$$C_{M_{ac,w}} = \left(C_{M_{ac_w}}\right)_{sections} + \left(C_{M_{ac_w}}\right)_{basic} = C_L \frac{(X_{ac} - X_{cg})}{\bar{c}} \quad (2.35)$$

Each term $\left(C_{M_{ac_w}}\right)_{sections}$ and $\left(C_{M_{ac_w}}\right)_{basic}$ can be expanded due to several

effects based on airfoil and wing properties. They are shown in the following equations.

$$\left(C_{M_{ac_w}}\right)_{sections} = \frac{2}{S\bar{c}} \left\{ \begin{array}{c} \int_0^{\frac{b}{2}} C_{m_{ac}}(y)c(y)^2dy + \\ \left(\int_0^{y_1} C_{m_{\delta_{f_1}}} c(y)^2dy\right)\delta_{f_1} + ... + \left(\int_{y_{N-1}}^{y_N} C_{m_{\delta_{f_N}}} c(y)^2dy\right)\delta_{f_N} \end{array} \right\} \tag{2.36}$$

$$\left(C_{M_{ac_w}}\right)_{basic} = \frac{2}{S\bar{c}} \left\{ \begin{array}{c} \int_0^{\frac{b}{2}} C_{lb,twist}(X_{ac,w} - X_{ac}(y))c(y)dy \\ +\int_0^{\frac{b}{2}} C_{lb,camber}(X_{ac,w} - X_{ac}(y))c(y)dy \\ + \left(\int_0^{\frac{b}{2}} C_{lb,\delta_{f_1}}(X_{ac,w} - X_{ac}(y))c(y)dy\right)\delta_{f_1} + ... \\ + \left(\int_0^{\frac{b}{2}} C_{lb,\delta_{f_N}}(X_{ac,w} - X_{ac}(y))c(y)dy\right)\delta_{f_N} \end{array} \right\} \tag{2.37}$$

Previous adaptive wing studies[16] have shown that it is convenient to define the adaptive flap deflections of $\{\delta_f\}$ be the sum of two parts: (1) the mean flap angle, $\bar{\delta}_f$, which is constant along span,, and (2) the variation about the mean, $\left\{\hat{\delta}_f\right\}$. Therefore, the adaptive flap deflection angle is a summation of these two, as shown in Eq. 2.38.

$$\{\delta_f\} = \bar{\delta}_f + \left\{\hat{\delta}_f\right\} \tag{2.38}$$

Then the mean flap deflection is computed by the following equation for enabling operation of the wing in the low-drag range of the airfoil for low profile drag.

$$\bar{\delta}_f = \frac{C_L - C_{L_{ideal}}}{2\sin\theta_f} \tag{2.39}$$

where θ_f is the angular coordinate for the hinge location $\frac{x_f}{c}$ in radians as described by Eq. 2.40.

$$\theta_f = \cos^{-1}\left(1 - 2\frac{x_f}{c}\right) \tag{2.40}$$

One of the biggest strength in his research was to decompose these two equations in terms of the mean flap angle and the variation angle. In order to do that, the terms due to the variation flap in the $\left(C_{M_{ac_w}}\right)_{sections}$ needs to be zero, which is shown as follows:

$$\left(\frac{2}{S\bar{c}}\int_0^{y_1} C_{m_{\hat{\delta}_{f_1}}} c(y)^2 dy\right)\hat{\delta}_{f_1} + ... + \left(\frac{2}{S\bar{c}}\int_{y_{N-1}}^{y_N} C_{m_{\hat{\delta}_{f_N}}} c(y)^2 dy\right)\hat{\delta}_{f_N} = 0 \tag{2.41}$$

This is called "weighting factor (WF) equation" which is solved when a calculation of the TE flap deflection angles is achieved. The details of the WF equation are provided in the next subsection.

Based on these methods, final forms of the Eqn 2.36 and Eqn 2.37 are shown as follows.

$$\left(C_{M_{ac_w}}\right)_{sections} = \frac{2}{S\bar{c}}\left\{\int_0^{\frac{b}{2}} C_{m_{ac}}(y)c(y)^2 dy + \left(\int_0^{\frac{b}{2}} C_{m_{\bar{\delta}_f}} c(y)^2 dy\right)\bar{\delta}_f\right\} \tag{2.42}$$

$$\left(C_{M_{ac_w}}\right)_{basic} = \frac{2}{S\bar{c}}\left\{\begin{array}{c}\left(\int_0^{\frac{b}{2}} C_{lb,\hat{\delta}_{f_1}}(X_{ac,w} - X_{ac}(y))c(y)dy\right)\hat{\delta}_{f_1} + ...+ \\ \left(\int_0^{\frac{b}{2}} C_{lb,\hat{\delta}_{f_N}}(X_{ac,w} - X_{ac}(y))c(y)dy\right)\hat{\delta}_{f_N}\end{array}\right\} \tag{2.43}$$

2.2 Procedure

The focus of the current problem is to solve for the optimal flap distribution resulting in minimized drag without and with constraints. There are several cases

according to the constraints setup, and solution procedures for each case are shown in the following subsections.

In the first subsection, a solution of the multiple TE flap deflection equation without constraints is described. Second part presents a calculation with a rolling moment control, which is a single constraint. Then the computation with multiple constraint is described. The last section describes the stuck-flap analysis and its calculation, which is the adaptive flap deflection computation when one of the flaps is stuck at some deflection angle.

2.2.1 Minimization of Induced Drag without Constraints

According to the requirements of the relative extrema in subsection 2.1.1, the first partial derivatives of the Eqn 2.31 were computed for variation flap angles, and set to zero as shown in the Eqn 2.44.

$$\left\{ \begin{array}{c} \frac{\partial C_{D_i}}{\partial \hat{\delta}_1} = 2C_L C_{D_{a1}} + 2C_{D_{11}}\hat{\delta}_1 + 2C_{D_{12}}\hat{\delta}_2 + \cdots + 2C_{D_{1N}}\hat{\delta}_N = 0 \\ \vdots \\ \frac{\partial C_{D_i}}{\partial \hat{\delta}_N} = 2C_L C_{D_{aN}} + 2C_{D_{NN}}\hat{\delta}_N + 2C_{D_{1N}}\hat{\delta}_1 + \cdots + 2C_{D_{(N-1)N}}\hat{\delta}_{N-1} = 0 \end{array} \right\} \tag{2.44}$$

These equations are simplified and rewritten in a matrix form as follows:

$$\begin{bmatrix} 2C_{D_{11}} & 2C_{D_{12}} & \cdots & 2C_{D_{1N}} \\ 2C_{D_{21}} & \cdots & & \vdots \\ \vdots & & \ddots & \vdots \\ 2C_{D_{N1}} & \cdots & \cdots & 2C_{D_{NN}} \end{bmatrix} \begin{Bmatrix} \hat{\delta}_1 \\ \hat{\delta}_2 \\ \vdots \\ \hat{\delta}_N \end{Bmatrix} = \begin{Bmatrix} -2C_L C_{D_{a1}} \\ -2C_L C_{D_{a2}} \\ \vdots \\ -2C_L C_{D_{aN}} \end{Bmatrix} \tag{2.45}$$

A square matrix with drag coefficients in the left hand side of the equation is referred to here as the "drag matrix". It is necessary to mention here that the drag matrix is a singular matrix. In other words, the Eqn 2.45 cannot be solved

with the matrix equation as shown. This is why the weighting factor equation is applied to this to obtain the unique solution of the flap deflections.

The wing C_L in the right hand side of the equation is the desired lift coefficient. A vector with flap deflections is the output of the system which is the adaptive flap deflections. Since the drag matrix and the right hand side vector can be computed, the final goal of the flap deflections is obtained after applying the weighting factor.

The weighting factor equation for the rolling moment constraint is now presented. Assuming that the flap to chord ratio being constants, the Eqn. 2.46 can be derived for non-constant chord distributions and different flap spans.

$$\bar{\delta_f} = \hat{\delta}_1 \cdot \frac{S_1}{S_{ref}} + \hat{\delta}_2 \cdot \frac{S_2}{S_{ref}} + \cdots + \hat{\delta}_N \cdot \frac{S_N}{S_{ref}} = \frac{C_L - C_{L_{ideal}}}{2sin\theta_f} \tag{2.46}$$

Now this weighting factor equation is applied to the system.

$$\begin{bmatrix} 2C_{D_{11}} & \cdots & 2C_{D_{1N}} \\ \vdots & \ddots & \vdots \\ 2C_{D_{N1}} & \cdots & 2C_{D_{NN}} \\ (\frac{S_1}{S_{ref}}) & \cdots & (\frac{S_N}{S_{ref}}) \end{bmatrix} \begin{Bmatrix} \hat{\delta}_1 \\ \vdots \\ \hat{\delta}_N \end{Bmatrix} = \begin{Bmatrix} -2C_L C_{D_{a1}} \\ \vdots \\ -2C_L C_{D_{aN}} \\ \bar{\delta_f} \end{Bmatrix} \tag{2.47}$$

It is convenient to use a Vortex Lattice Method (VLM) or a panel method for computing the elements of the drag matrix and the RHS. For this research, a code called AVL (Athena Vortex Lattice)[24] is used. Using the AVL, first of all, the additional case was run and the lift and downwash distributions were obtained. Then all basic cases with each flap deflections were computed.

Because of the use of AVL, the drag matrix with the drag coefficients as well as ones in the right hand side can be computed based on Eqn 2.28, Eqn 2.29, Eqn 2.30.

2.2.2 Minimization of Induced Drag with Rolling Moment Constraint

In order to utilize Eqn 2.7 for the adaptive wing with the basic and additional loading theory, the Eqn 2.18 is applied as shown below.

$$C_R = -\frac{1}{S_{ref} b_{ref}} \{ \int_{-\frac{b}{2}}^{\frac{b}{2}} c C_{lb} y dy + \int_{-\frac{b}{2}}^{\frac{b}{2}} c C_L C_{la,1} y dy \} \tag{2.48}$$

The additional distribution is a lift distribution with zero flap deflections and zero spanwise twist on the wing. This means that the distribution is symmetric on both sides of the wing. Therefore, the additional distribution has no contribution to a production of the rolling moment. Also, this research focuses on the TE flaps but not any twist or camber change along the span based on Eqn 2.19. Therefore the Eqn 2.48 is rewritten as follows.

$$C_R = -\frac{1}{S_{ref} b_{ref}} \{ \int_{-\frac{b}{2}}^{\frac{b}{2}} c C_{lb,flap} y dy \} \tag{2.49}$$

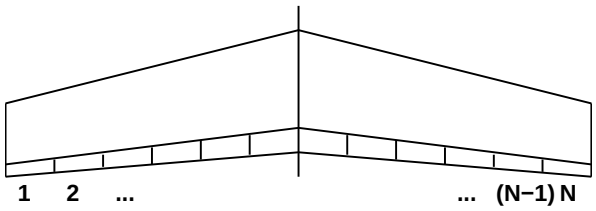

Figure 2.4: Adaptive flaps (top view).

Throughout this research the multiple TE flaps are numbered as shown in Figure 2.4 which is numbered for the whole span. According to this setup, the rolling moment equation (Eqn 2.49) is expressed as:

$$C_R = -\frac{1}{S_{ref} b_{ref}} \{ (\int_{-\frac{b}{2}}^{\frac{b}{2}} cC_{lb,\delta_1} y dy)\delta_1 + \cdots + (\int_{-\frac{b}{2}}^{\frac{b}{2}} cC_{lb,\delta_N} y dy)\delta_N \} \tag{2.50}$$

According to Eqn 2.38, the flap deflection is decomposed as mean and variation terms. Also, the mean is constant along span and therefore, it does not have a contribution in generating the rolling moment. Therefore, the equation is rewritten as follows.

$$C_R = -\frac{1}{S_{ref} b_{ref}} \{ (\int_{-\frac{b}{2}}^{\frac{b}{2}} cC_{lb,\hat{\delta}_1} y dy)\hat{\delta}_1 + \cdots + (\int_{-\frac{b}{2}}^{\frac{b}{2}} cC_{lb,\hat{\delta}_N} y dy)\hat{\delta}_N \} \tag{2.51}$$

The Eqn 2.51 is a final expression of the rolling moment equation due to the multiple TE flaps. This equation is then used to as a constraint of the system of the multiple TE flaps. The mean flap angle, which was explained in the previous section, is a function of the weighting factor which shows the relative effectiveness of each flaps.

Using the method of Lagrange multipliers (λ), as explained in Bryson and Ho,[19] the constraint equation, g, is the rolling moment equation of Eqn 2.51.

$$g(x_i) = (C_R)_{desired} + \frac{1}{S_{ref} b_{ref}} \{ (\int_{-\frac{b}{2}}^{\frac{b}{2}} cC_{lb,\hat{\delta}_1} y dy)\hat{\delta}_1 + \cdots + (\int_{-\frac{b}{2}}^{\frac{b}{2}} cC_{lb,\hat{\delta}_N} y dy)\hat{\delta}_N \} = 0 \tag{2.52}$$

Finally, this method of Lagrange multipliers for the constraint is applied to the system matrix of Eqn 2.47.

$$\begin{bmatrix} 2C_{D_{11}} & \cdots & 2C_{D_{1N}} & \frac{1}{Sb}\int_{-\frac{b}{2}}^{\frac{b}{2}} cC_{l_b,\hat{\delta}_1} ydy \\ \vdots & \ddots & \vdots & \vdots \\ 2C_{D_{N1}} & \cdots & 2C_{D_{NN}} & \frac{1}{Sb}\int_{-\frac{b}{2}}^{\frac{b}{2}} cC_{l_b,\hat{\delta}_N} ydy \\ (\frac{S_1}{S_{ref}}) & \cdots & (\frac{S_N}{S_{ref}}) & 0 \\ -\frac{1}{Sb}\int_{-\frac{b}{2}}^{\frac{b}{2}} cC_{l_b,\hat{\delta}_1} ydy & \cdots & -\frac{1}{Sb}\int_{-\frac{b}{2}}^{\frac{b}{2}} cC_{l_b,\hat{\delta}_N} ydy & 0 \end{bmatrix} \begin{Bmatrix} \hat{\delta}_1 \\ \vdots \\ \hat{\delta}_N \\ \lambda \end{Bmatrix}$$
$$= \begin{Bmatrix} -2C_L C_{D_{a1}} \\ \vdots \\ -2C_L C_{D_{aN}} \\ \bar{\delta_f} \\ (C_R)_{desired} \end{Bmatrix} \tag{2.53}$$

This is the final expression of the matrix equation with constraint. Then each of the system with and without the constraints (Eqn 2.47, Eqn 2.53) are solved for various wing configurations. Those results are shown in the next chapter.

2.2.3 Minimization of Induced Drag with Pitch and Roll Constraints

In this section, the equations for dual constraints on rolling and pitching moment are presented. The weighting factor equation is adapted from the work of Cusher and Gopalarathnam.[17] Just like the rolling moment constraint, the weighting factor for pitching moment of Eqn 2.41 is applied to the system.

$$\begin{bmatrix} 2C_{D_{11}} & \cdots & 2C_{D_{1N}} \\ \vdots & \ddots & \vdots \\ 2C_{D_{N1}} & \cdots & 2C_{D_{NN}} \\ \frac{2}{S\bar{c}}\int_0^{y_1} C_{m_{\hat{\delta}_{f_1}}} c(y)^2 dy & \cdots & \frac{2}{S\bar{c}}\int_{y_{N-1}}^{y_N} C_{m_{\hat{\delta}_{f_N}}} c(y)^2 dy \end{bmatrix} \begin{Bmatrix} \hat{\delta}_1 \\ \vdots \\ \hat{\delta}_N \end{Bmatrix} = \begin{Bmatrix} -2C_L C_{D_{a1}} \\ \vdots \\ -2C_L C_{D_{aN}} \\ 0 \end{Bmatrix} \tag{2.54}$$

This is a system without constraints from pitching moment standpoint. This system will provide a very similar output with the one by Eqn 2.47.

The system with a single constraint of pitching moment is determined based on Eqn 2.2 and Eqn 2.43.

$$\begin{bmatrix} 2C_{D_{11}} & \cdots & 2C_{D_{1N}} & -\frac{2}{S\bar{c}}\int_0^{\frac{b}{2}} C_{lb,\hat{\delta}_{f_1}} \Delta x c dy \\ \vdots & \ddots & \vdots & \vdots \\ 2C_{D_{N1}} & \cdots & 2C_{D_{NN}} & -\frac{2}{S\bar{c}}\int_0^{\frac{b}{2}} C_{lb,\hat{\delta}_{f_N}} \Delta x c dy \\ \frac{2}{S\bar{c}}\int_0^{y_1} C_{m_{\hat{\delta}_{f_1}}} c^2 dy & \cdots & \frac{2}{S\bar{c}}\int_{y_{N-1}}^{y_N} C_{m_{\hat{\delta}_{f_N}}} c^2 dy & 0 \\ \frac{2}{S\bar{c}}\int_0^{\frac{b}{2}} C_{lb,\hat{\delta}_{f_1}} \Delta x c dy & \cdots & \frac{2}{S\bar{c}}\int_0^{\frac{b}{2}} C_{lb,\hat{\delta}_{f_N}} \Delta x c dy & 0 \end{bmatrix} \begin{Bmatrix} \hat{\delta}_1 \\ \vdots \\ \hat{\delta}_N \\ \lambda \end{Bmatrix}$$
$$= \begin{Bmatrix} -2C_L C_{D_{a1}} \\ \vdots \\ -2C_L C_{D_{aN}} \\ 0 \\ \left(C_{M_{ac_w}}\right)_{basic} \end{Bmatrix} \tag{2.55}$$

In the equation, Δx represents the term $X_{ac,w} - X_{ac}(y)$. There are two ways of computing its output based on cases of reducing the induced drag only and the one with profile drag. Cusher referred to these as Scheme A and Scheme B.

First of all, the static margin of an aircraft is set as well as a desired wing C_L. Then the wing pitching moment is determined by Eqn 2.33.

For the Scheme A, solve Eqn 2.54 for variation angles. Then the angles are

substituted into the Eqn 2.43 to obtain $(C_{M_{ac_w}})_{basic}$. Then the $(C_{M_{ac_w}})_{sections}$ can be computed by Eqn 2.35. Finally the mean flap angle is found by Eqn 2.42 to obtain the final flap deflection angles by Eqn 2.38.

For the Scheme B, the $C_{L_{ideal}}$ is determined due to the airfoil selection. From the obtained mean flap angle, the $(C_{M_{ac_w}})_{sections}$ is computed by the Eqn 2.42. This enables to calculate $(C_{M_{ac_w}})_{basic}$ by Eqn 2.35. Finally the system of Eqn 2.55 is computed to obtain the total flap deflections of $\{\delta_f\}$.

Since the single constraint of rolling moment has been applied to the system as well as the pitching moment, two constraint of pitch and roll are applied to the system so that it compute the adaptive flap deflections based on these two constraints.

The multiple constraints are achieved based on the Eqn 2.2. To able to obtain output for Scheme A and B of the pitching moment constraint, the rolling moment equation is applied to both of Eqn 2.54 and Eqn 2.55.

$$\begin{bmatrix} 2C_{D_{11}} & \dots & 2C_{D_{1N}} & R_1 \\ \vdots & \ddots & \vdots & \vdots \\ 2C_{D_{N1}} & \dots & 2C_{D_{NN}} & R_N \\ \frac{2}{S\bar{c}}\int_0^{y_1} C_{m_{\hat{\delta}_{f_1}}} c^2 dy & \dots & \frac{2}{S\bar{c}}\int_{y_{N-1}}^{y_N} C_{m_{\hat{\delta}_{f_N}}} c^2 dy & 0 \\ -R_1 & \cdots & -R_N & 0 \end{bmatrix} \cdot \begin{Bmatrix} \hat{\delta}_1 \\ \vdots \\ \hat{\delta}_N \\ \lambda_1 \end{Bmatrix}$$
$$= \begin{Bmatrix} -2C_L C_{D_{a1}} \\ \vdots \\ -2C_L C_{D_{aN}} \\ 0 \\ (C_R)_{basic} \end{Bmatrix} \tag{2.56}$$

$$\begin{bmatrix} 2C_{D_{11}} & \dots & 2C_{D_{1N}} & R_1 & -P_1 \\ \vdots & \ddots & \vdots & \vdots & \vdots \\ 2C_{D_{N1}} & \dots & 2C_{D_{NN}} & R_N & -P_N \\ \frac{2}{S\bar{c}}\int_0^{y_1} C_{m_{\hat{\delta}_{f_1}}} c^2 dy & \dots & \frac{2}{S\bar{c}}\int_{y_{N-1}}^{y_N} C_{m_{\hat{\delta}_{f_N}}} c^2 dy & 0 & 0 \\ -R_1 & \cdots & -R_N & 0 & 0 \\ P_1 & \dots & P_N & 0 & 0 \end{bmatrix} \cdot \begin{Bmatrix} \hat{\delta}_1 \\ \vdots \\ \hat{\delta}_N \\ \lambda_1 \\ \lambda_2 \end{Bmatrix}$$
$$= \begin{Bmatrix} -2C_L C_{D_{a1}} \\ \vdots \\ -2C_L C_{D_{aN}} \\ 0 \\ (C_R)_{basic} \\ \left(C_{Mac_w}\right)_{basic} \end{Bmatrix} \tag{2.57}$$

In which $R_n = \frac{1}{Sb}\int_{-\frac{b}{2}}^{\frac{b}{2}} cC_{l_b,\hat{\delta}_n} y dy$, and $P_n = -\frac{2}{S\bar{c}}\int_0^{\frac{b}{2}} C_{lb,\hat{\delta}_{f_n}} \Delta x c dy$ for equation simplicity.

These two equations are used for each scheme according to the previous sections of Sec 2.2.2 with the rolling moment requirement from Sec 2.1.2.

2.2.4 Optimum Loading with a Control Failure

The system matrix can also be solved when one of the flaps is stuck at a known angle due to control failure. For this research only a single constraint of rolling moment is considered.

First of all, the stuck flap was chosen as the xth which is between 1st and Nth in the total number of N TE flaps. Noting that $\frac{\partial C_{D_i}}{\partial \hat{\delta}_x}$ is not set to zero, the system matrix of Eqn 2.47 is modified as follows.

$$\begin{gathered}
2C_{D_{11}}(\hat{\delta}_1) + \cdots + 2C_{D_{1x}}(\hat{\delta}_x) + \cdots + 2C_{D_{1N}}(\hat{\delta}_N) = -2C_L C_{D_{a1}} \\
\vdots \\
2C_{D_{(x-1)1}}(\hat{\delta}_1) + \cdots + 2C_{D_{(x-1)x}}(\hat{\delta}_x) + \cdots + 2C_{D_{(x-1)N}}(\hat{\delta}_N) = -2C_L C_{D_{a(x-1)}} \\
2C_{D_{(x+1)1}}(\hat{\delta}_1) + \cdots + 2C_{D_{(x+1)x}}(\hat{\delta}_x) + \cdots + 2C_{D_{(x+1)N}}(\hat{\delta}_N) = -2C_L C_{D_{a(x+1)}} \\
\vdots \\
2C_{D_{N1}}(\hat{\delta}_1) + \cdots + 2C_{D_{Nx}}(\hat{\delta}_x) + \cdots + 2C_{D_{NN}}(\hat{\delta}_N) = -2C_L C_{D_{aN}} \\
\tfrac{S_1}{S_{ref}}(\hat{\delta}_1) + \cdots + \tfrac{S_x}{S_{ref}}(\hat{\delta}_x) + \cdots + \tfrac{S_N}{S_{ref}}(\hat{\delta}_N) = \bar{\delta_f}
\end{gathered} \tag{2.58}$$

Since the $(\hat{\delta_x})$ is known, all the terms including this are moved to the right hand side of the equation.

$$
\begin{aligned}
2C_{D_{11}}(\hat{\delta}_1) + \cdots + 2C_{D_{1N}}(\hat{\delta}_N) &= -2C_L C_{D_{a1}} - 2C_{D_{1x}}(\hat{\delta}_x) \\
&\vdots \\
2C_{D_{(x-1)1}}(\hat{\delta}_1) + \cdots + 2C_{D_{(x-1)N}}(\hat{\delta}_N) &= -2C_L C_{D_{a(x-1)}} - 2C_{D_{(x-1)x}}(\hat{\delta}_x) \\
2C_{D_{(x+1)1}}(\hat{\delta}_1) + \cdots + 2C_{D_{(x+1)N}}(\hat{\delta}_N) &= -2C_L C_{D_{a(x+1)}} - 2C_{D_{(x+1)x}}(\hat{\delta}_x) \\
&\vdots \\
2C_{D_{N1}}(\hat{\delta}_1) + \cdots + 2C_{D_{NN}}(\hat{\delta}_N) &= -2C_L C_{D_{aN}} - 2C_{D_{Nx}}(\hat{\delta}_x) \\
\tfrac{S_1}{S_{ref}}(\hat{\delta}_1) + \cdots + \tfrac{S_N}{S_{ref}}(\hat{\delta}_N) &= \bar{\delta_f} - \tfrac{S_x}{S_{ref}}(\hat{\delta}_x)
\end{aligned}
\tag{2.59}
$$

These equations are now reshaped as the matrix form as follows.

$$
\begin{bmatrix}
2C_{D_{11}} & \cdots & 2C_{D_{1x-1}} & 2C_{D_{1x+1}} & \cdots & 2C_{D_{1N}} \\
\vdots & \cdots & \vdots & \vdots & \cdots & \vdots \\
2C_{D_{(x-1)1}} & \cdots & 2C_{D_{(x-1)x-1}} & 2C_{D_{(x-1)x+1}} & \cdots & 2C_{D_{(x-1)N}} \\
2C_{D_{(x+1)1}} & \cdots & 2C_{D_{(x+1)x-1}} & 2C_{D_{(x+1)x+1}} & \cdots & 2C_{D_{(x+1)N}} \\
\vdots & \cdots & \vdots & \vdots & \cdots & \vdots \\
2C_{D_{N1}} & \cdots & 2C_{D_{Nx-1}} & 2C_{D_{Nx+1}} & \cdots & 2C_{D_{NN}} \\
(\frac{S_1}{S_{ref}}) & \cdots & (\frac{S_{x-1}}{S_{ref}}) & (\frac{S_{x+1}}{S_{ref}}) & \cdots & (\frac{S_N}{S_{ref}})
\end{bmatrix}
\begin{Bmatrix}
\hat{\delta}_1 \\ \vdots \\ \hat{\delta}_{x-1} \\ \hat{\delta}_{x+1} \\ \vdots \\ \hat{\delta}_N
\end{Bmatrix}
$$

$$
= \begin{Bmatrix}
-2C_L C_{D_{a1}} - 2C_{D_{1x}}(\hat{\delta}_x) \\
\vdots \\
-2C_L C_{D_{a(x-1)}} - 2C_{D_{(x-1)x}}(\hat{\delta}_x) \\
-2C_L C_{D_{a(x+1)}} - 2C_{D_{(x+1)x}}(\hat{\delta}_x) \\
\vdots \\
-2C_L C_{D_{aN}} - 2C_{D_{Nx}}(\hat{\delta}_x) \\
\bar{\delta_f} - \frac{S_x}{S_{ref}}(\hat{\delta}_x)
\end{Bmatrix}
\tag{2.60}
$$

The size of the LHS matrix is $(N) \times (N-1)$, the output deflection vector size is $(N-1) \times 1$, and the RHS vector is $(N) \times 1$. Therefore, the system can be

solved.

For a case with a rolling moment control, the constraint equation is simply added to this newly organized matrix as follows. In the equation R_n represents the term $\frac{1}{Sb}\int_{-\frac{b}{2}}^{\frac{b}{2}} cC_{l_b,\hat{\delta}_n} ydy$.

$$\begin{bmatrix} 2C_{D_{11}} & \cdots & 2C_{D_{1x-1}} & 2C_{D_{1x+1}} & \cdots & 2C_{D_{1N}} & R_1 \\ \vdots & \cdots & \vdots & \vdots & \cdots & \vdots & \vdots \\ 2C_{D_{(x-1)1}} & \cdots & 2C_{D_{(x-1)x-1}} & 2C_{D_{(x-1)x+1}} & \cdots & 2C_{D_{(x-1)N}} & R_{x+1} \\ 2C_{D_{(x+1)1}} & \cdots & 2C_{D_{(x+1)x-1}} & 2C_{D_{(x+1)x+1}} & \cdots & 2C_{D_{(x+1)N}} & R_{x-1} \\ \vdots & \cdots & \vdots & \vdots & \cdots & \vdots & \vdots \\ 2C_{D_{N1}} & \cdots & 2C_{D_{Nx-1}} & 2C_{D_{Nx+1}} & \cdots & 2C_{D_{NN}} & R_N \\ (\frac{S_1}{S_{ref}}) & \cdots & (\frac{S_{x-1}}{S_{ref}}) & (\frac{S_{x+1}}{S_{ref}}) & \cdots & (\frac{S_N}{S_{ref}}) & 0 \\ -R_1 & \cdots & -R_{x-1} & -R_{x+1} & \cdots & -R_N & 0 \end{bmatrix} \begin{Bmatrix} \hat{\delta}_1 \\ \vdots \\ \hat{\delta}_{x-1} \\ \hat{\delta}_{x+1} \\ \vdots \\ \hat{\delta}_N \\ \lambda \end{Bmatrix}$$

$$= \begin{Bmatrix} -2C_L C_{D_{a1}} - 2C_{D_{1x}}(\hat{\delta}_x) \\ \vdots \\ -2C_L C_{D_{a(x-1)}} - 2C_{D_{(x-1)x}}(\hat{\delta}_x) \\ -2C_L C_{D_{a(x+1)}} - 2C_{D_{(x+1)x}}(\hat{\delta}_x) \\ \vdots \\ -2C_L C_{D_{aN}} - 2C_{D_{Nx}}(\hat{\delta}_x) \\ \bar{\delta_f} - \frac{S_x}{S_{ref}}(\hat{\delta}_x) \\ (C_R)_{basic} + R_x \end{Bmatrix} \tag{2.61}$$

Therefore, all the elements of the drag matrix are known as well as the elements of the right hand side vector. This system can then be solved for the controllable TE flap deflection angles.

If the number of stuck flaps are more than two, then the system matrix can also be solved following the same steps with two known TE deflection angles. For this research, again, only the one stuck flap case was analyzed.

Chapter 3

Results

In this chapter, results for different test cases are presented and discussed. To obtain the results, a few example wings are used, with dimensions and airfoil selections shown in the Section 3.1.

Section 3.2 shows the results with a single constraint of rolling moment. Section 3.3 shows the results for two constraints of rolling and pitching moments. Section 3.4 shows some results for a single constraint of the rolling moment with a stuck flap as an example of control failure.

3.1 Test Cases

Three kinds of wing shapes are used as examples for this research. The first wing is a straight-tapered wing with the taper-ratio (λ) of 0.7, shown in Fig. 3.1. This wing was used for a case of single constraint of rolling moment. The next two wings are the swept-tapered-wing with the sweep ($\Lambda_{c/4}$) of 20 degrees and 35 degrees with the same taper-ratio, shown in Fig. 3.2. These two wings were used for both single and multiple constraint cases.

Using these two wings, a hypothetical tailless aircraft was used as an sample platform with characteristics displayed in Table 3.1. These characteristics were determined based on the tailless aircraft analysis by Cusher and Gopalarathnam.[17]

Table 3.1: Assumed parameter values for example tailless aircraft.

Static Parameters	Value
Gross weight (W)	14,200 N
	(3,200 lbf)
Mean aerodynamic chord ($\bar{c}$)	1.01 m
	(3.31 ft)
Reference area (S)	12.0 m^2
	(130 ft^2)
Wing aspect ratio (AR)	12
Static margin (SM)	10 % $\bar{c}$
Number of half-span TE flaps (N)	5
Flap-to-chord ratio (all flaps)	0.2
Variable Parameters	**Value**
$\frac{1}{4}$ *chord* sweep angle ($\Lambda_{c/4}$)	20 deg
	35 deg
Airfoil section	NLF0824 ($CAMBERED$)
	($C_{m_0} = -0.0802$)
	Reflex055 ($REFLEXED$)
	($C_{m_0} = 0.055$)

For each wing shape, two different airfoils were used which were the same airfoils used in Ref. 17. The first airfoil is a cambered NLF airfoil which has a zero lift pitching moment coefficient (C_{m_0}) of -0.0802, and is labeled $CAMBERED$. This airfoil has a well defined low drag range. The second airfoil is a reflexed airfoil which was designed to have a positive C_{m_0} value of 0.055, and is named $REFLEXED$. Figures 3.3 and 3.4 display the properties of these airfoils as analyzed by XFOIL[25] calculated at a $Re\sqrt{C_l}$ of three million, as well as their corresponding geometries.

Based on these wing and airfoil selections, there are four example cases for a single constraint and four cases for multiple constraints case. Example Case $\#1-1$ is the $CAMBERED$ airfoil for a straight-tapered wing. Example Case $\#1-2$ is the $CAMBERED$ airfoil at $\Lambda_{c/4} = 35$ deg of wing sweep. Example Case $\#1-3$ is the $REFLEXED$ airfoil for a straight-tapered wing. Example

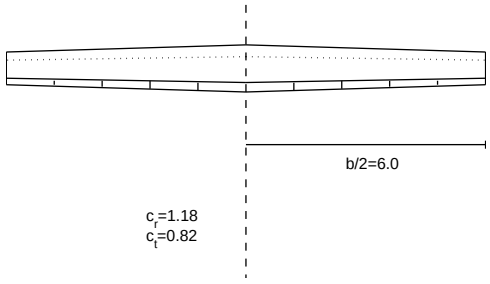

Figure 3.1: Example planform for unswept tapered wing with 5 TE flaps per half span.

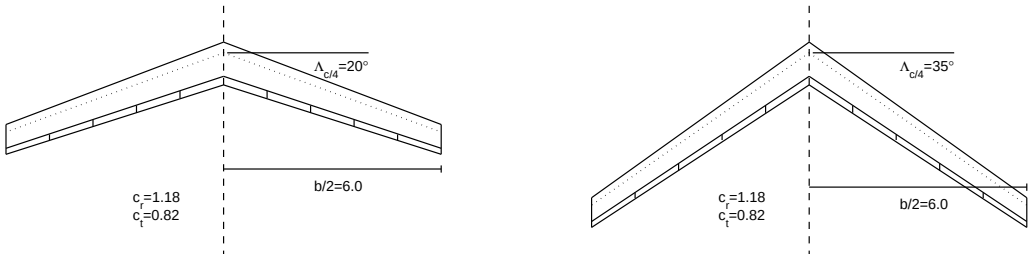

(a) (b)

Figure 3.2: Wing planform for swept tapered wing with 5 TE flaps per half span: (a) $\Lambda_{c/4}$ of 20 degrees and (b) $\Lambda_{c/4}$ of 35 degrees.

Case $\#1-4$ is the $REFLEXED$ airfoil with $\Lambda_{c/4} = 35$ deg of sweep. For each of these cases, the desired rolling moment coefficient values were set to C_R=0.02 and C_R=0.04 respectively. These desired values of C_R were determined as the rolling-moment coefficients for a generic transport aircraft with 5 deg and 10 deg aileron deflections.

For the multiple constraint case, two examples are studied. Example Case $\#2-1$ is the $CAMBERED$ airfoil at $\Lambda_{c/4} = 35$ deg. Example Case $\#2-2$ is the $REFLEXED$ airfoil at $\Lambda_{c/4} = 20$ deg. Each case were applied for both $SchemeA$ and $SchemeB$ which is shown in Cusher[17] with the two rolling moment coefficient values. For the supplemental analysis of a stuck flap in Sec. 3.4, only the straight-tapered wing with $CAMBERED$ airfoil is studied. However, two flaps were chosen as the stuck flaps and each case of data was taken with zero and 10 degrees of the flap deflections. The two flaps were, one at the left wing

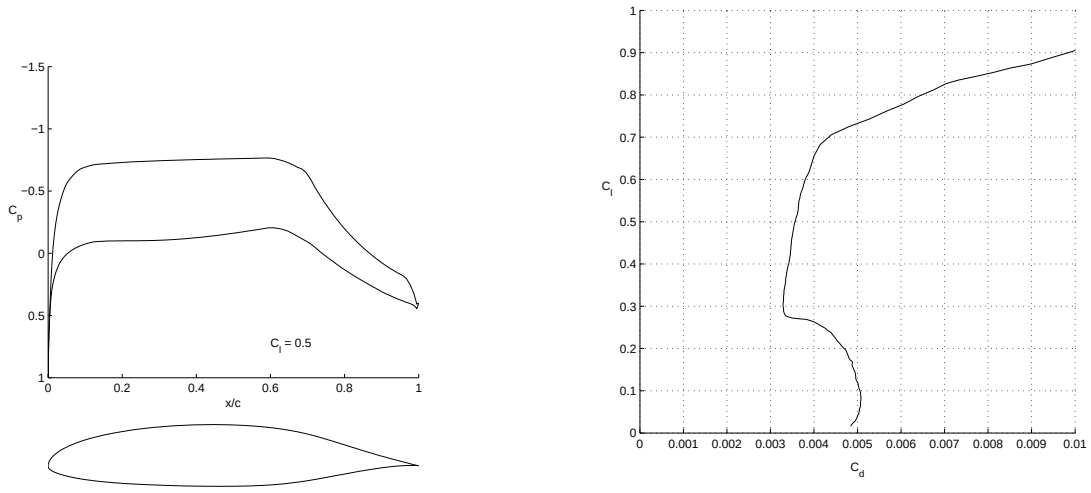

(a) (b)

Figure 3.3: $CAMBERED$ airfoil: (a) Geometry and C_p distribution and (b) drag polar at $Re\sqrt{C_l}$ of three million.

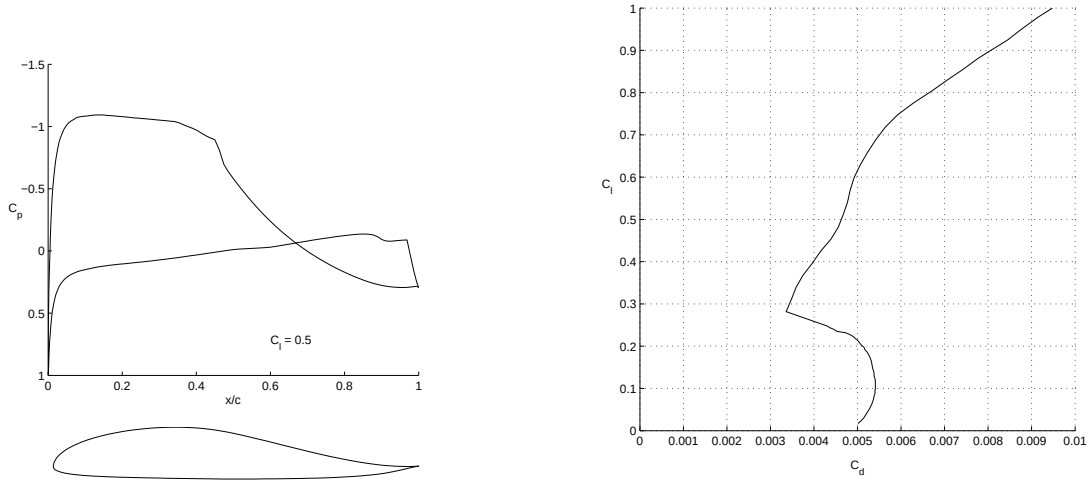

(a) (b)

Figure 3.4: $REFLEXED$ airfoil: (a) Geometry and C_p distribution and (b) drag polar at $Re\sqrt{C_l}$ of three million.

tip, which is called *Flap*.1, and another located next to the wing root on the right hand side of the wing, which is named *Flap*.6. For each case the two rolling moment coefficient values were applied.

3.2 Rolling Moment Constraint

3.2.1 Example Case #1 − 1

The first case is the $CAMBERED$ airfoil used on the straight-tapered wing planform with no sweep angle shown in Fig. 3.1. The C_l distribution and drag polar for each flap are shown in the Fig. 3.5. The desired rolling moment coefficient, $C_{R_{desired}}$, is 0.02. Three C_l distributions for the different wing C_L values of 0.2, 0.5, 0.8 are shown in the figure. For each distribution the total induced drag, rolling moment coefficients, and mean flap deflection angles are shown on the left in the plot. The distribution shown as a dash-dot line is the elliptical distribution. This distribution has no rolling moment because it is symmetric about the wing root. The C_l distribution with a solid line is the optimum distribution which was described in Sec. 2.1.2. The distribution with circle markers is the adapted distribution achieved by using the multiple TE flap deflections. For each flapped portion of the wing, the drag polar for that flap angle is plotted, to check if that portion of the wing is operating within the drag bucket of the airfoil.

It is clear that the adapted distribution is very close to the optimum serves to verify the theory of induced drag minimization with the rolling moment constraint. The flap angles are listed in Fig. 3.5 for each C_L. It is seen the flap angles are all moderate and not high enough for flow separation to be a concern. It is also seen that each portion of the wing is operating within the corresponding low-drag range, resulting in minimum profile drag in addition to minimum induced drag. Figure 3.6 shows a similar plot for $C_{R_{desired}}$=0.04.

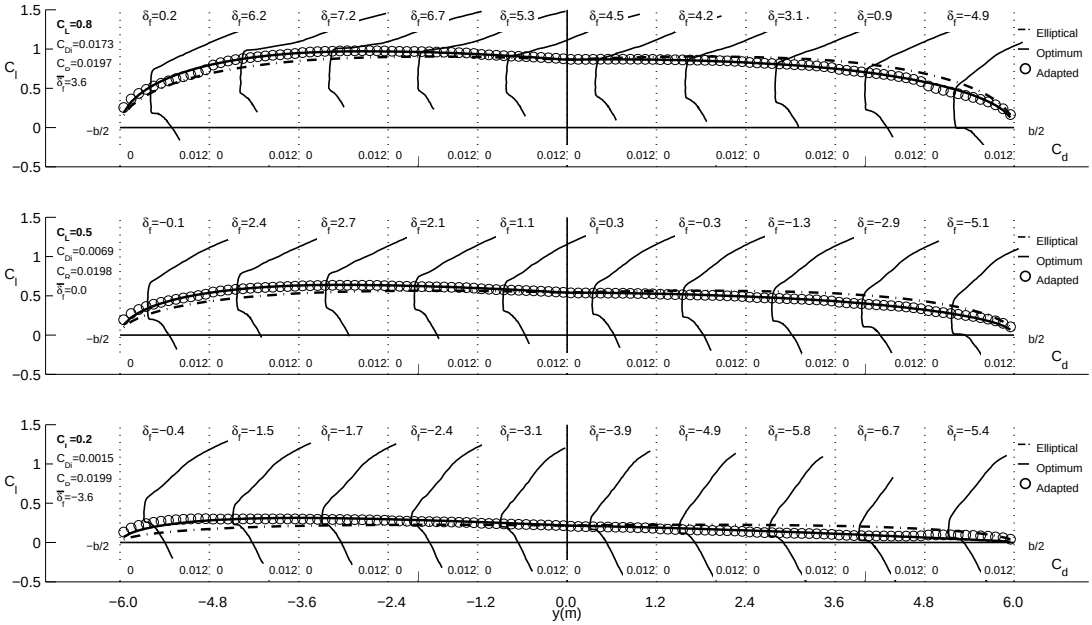

Figure 3.5: Spanwise C_l distributions with flap-section drag polars and optimal C_l distributions with $C_{R_{desired}}$=0.02 for Example Case #1 − 1.

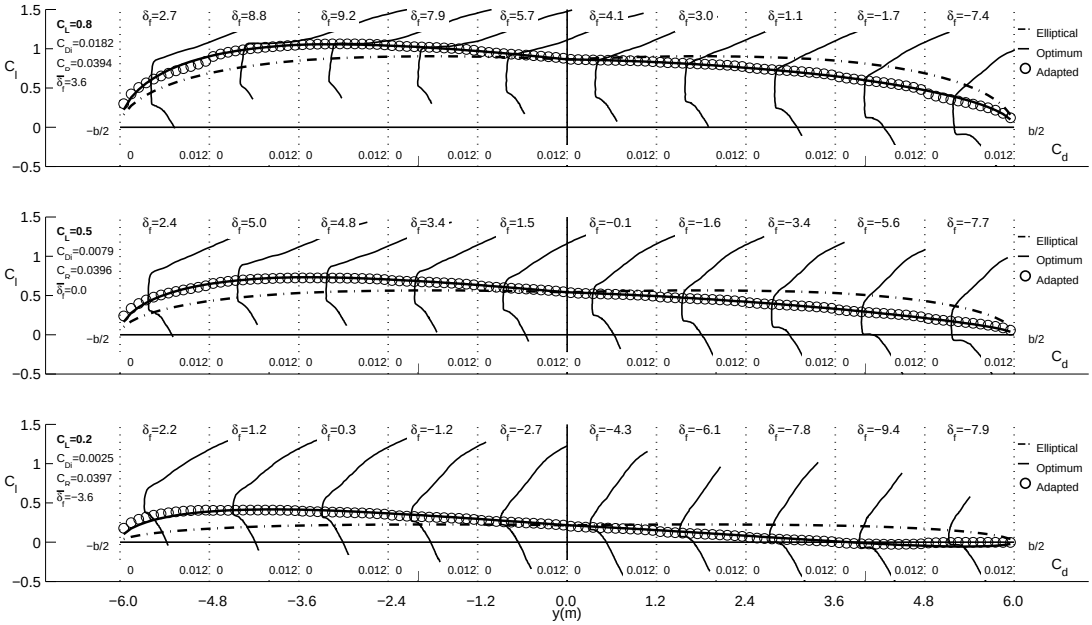

Figure 3.6: Spanwise C_l distributions with flap-section drag polars and optimal C_l distributions with $C_{R_{desired}}$=0.04 for Example Case #1 − 1.

Comparing the Fig. 3.5 and Fig. 3.6 it is found that a larger value of $C_{R_{desired}}$ causes more induced drag due to a greater deviation from the elliptical lift distribution. However, the theory is based on the minimization of the induced drag with the rolling moment control, so the amount of the drag increased is kept to a minimum.

3.2.2 Example Case $\#1-2$

The next case discussed is the $CAMBERED$ airfoil used on the swept wing of $\Lambda_{c/4} = 35$ deg. The following plots in Fig. 3.7 Fig. 3.8 are the C_l distributions with the drag polars for each corresponding flap each $C_{R_{desired}}$=0.02 and $C_{R_{desired}}$=0.04.

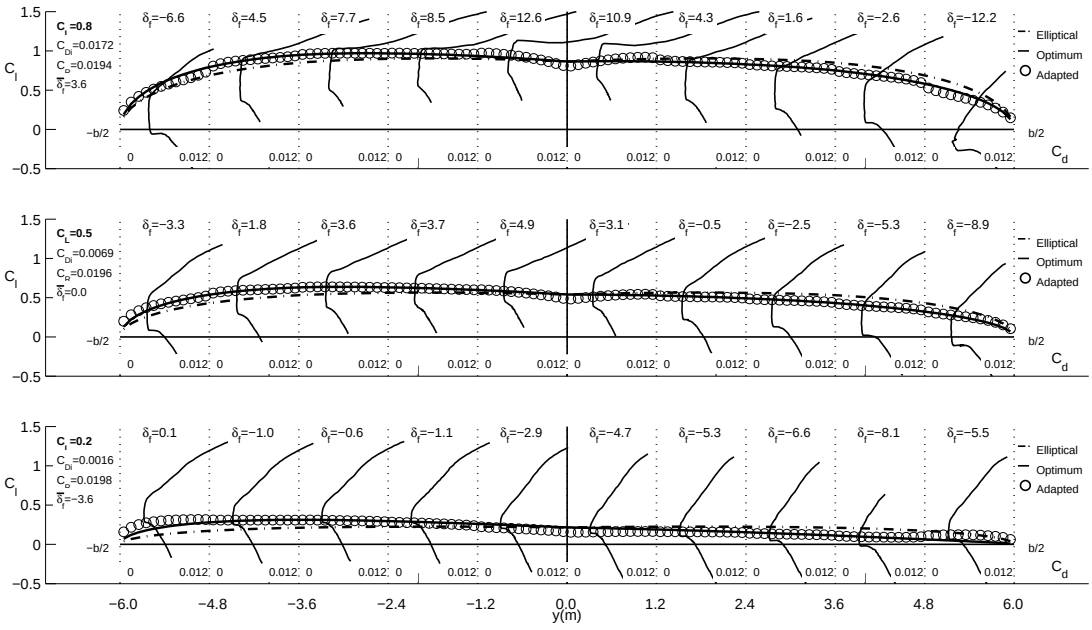

Figure 3.7: Spanwise C_l distributions with flap-section drag polars and optimal C_l distributions with $C_{R_{desired}}$=0.02 for Example Case $\#1-2$.

As it can be seen in those plots, the distributions for each rolling moment values are similar to the the Example Case $\#1-1$. The maximum deflection was δ_f=-15.0 deg at the $C_L = 0.8$ with $C_{R_{desired}}$=0.04. This is due to a shape of the wing. In other words, the straight-tapered wing achieves the optimum distribution

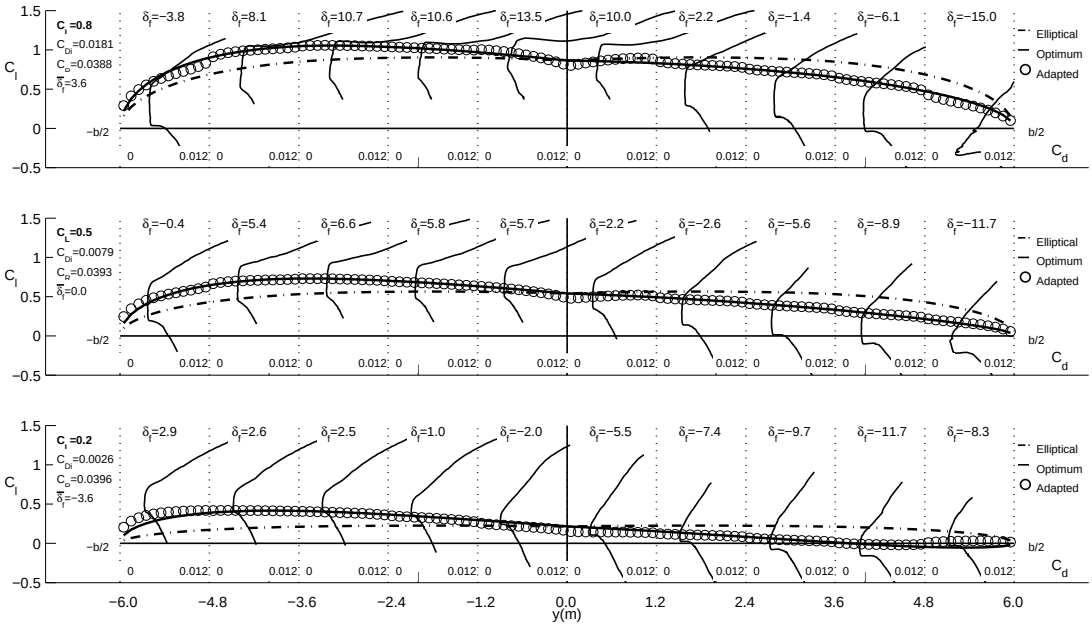

Figure 3.8: Spanwise C_l distributions with flap-section drag polars and optimal C_l distributions with $C_{R_{desired}}$=0.04 for Example Case #1 − 2.

easily because the wing shape is much close to the elliptical wing than swept wing. However, this amount of deflection is acceptable and the adaptive distributions were successfully obtained.

3.2.3 Example Case #1 − 3

For this case the same wing geometry with the Example Case#1 − 1 of straight-tapered wing was used but different airfoil which is the $REFLEXED$ airfoil. The following plots of Fig. 3.9 Fig. 3.10 are the C_l distributions with the drag polars for this case.

It is found that the behavior of the drag polar is somewhat different with the $CAMBERED$ airfoils in the Example Cases of #1 − 1 and #1 − 2. As already shown in the previous cases, the $CAMBERED$ airfoil has a well-defined drag bucket. The $REFLEXED$ airfoil, however, has smaller drag bucket and the upper edge of the bucket is not very well-defined compared with the $CAMBERED$

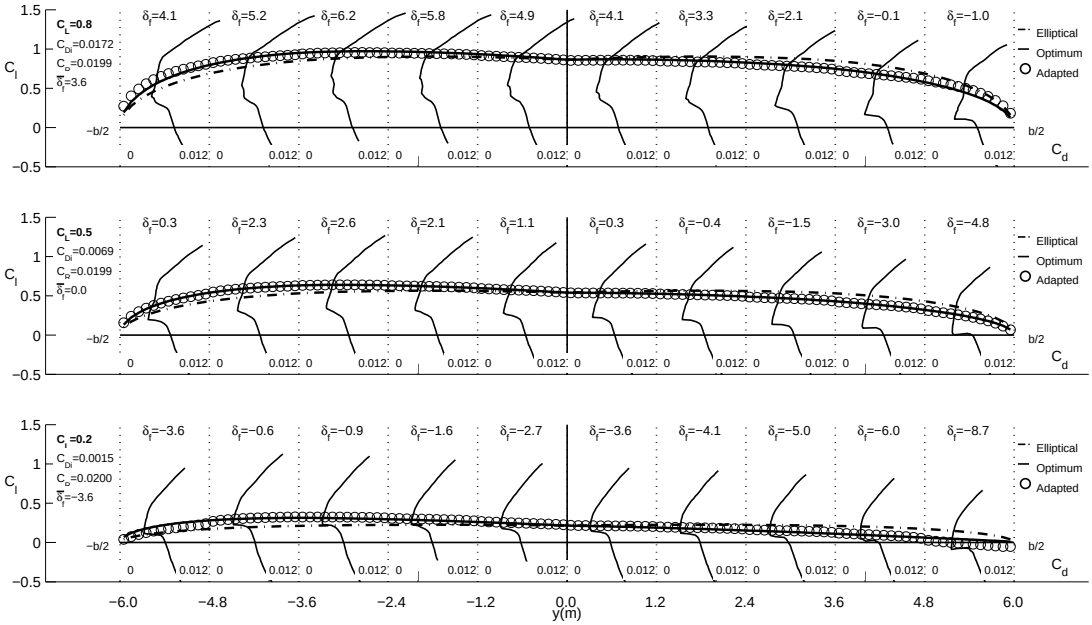

Figure 3.9: Spanwise C_l distributions with flap-section drag polars and optimal C_l distributions with $C_{R_{desired}}$=0.02 for Example Case #1 − 3.

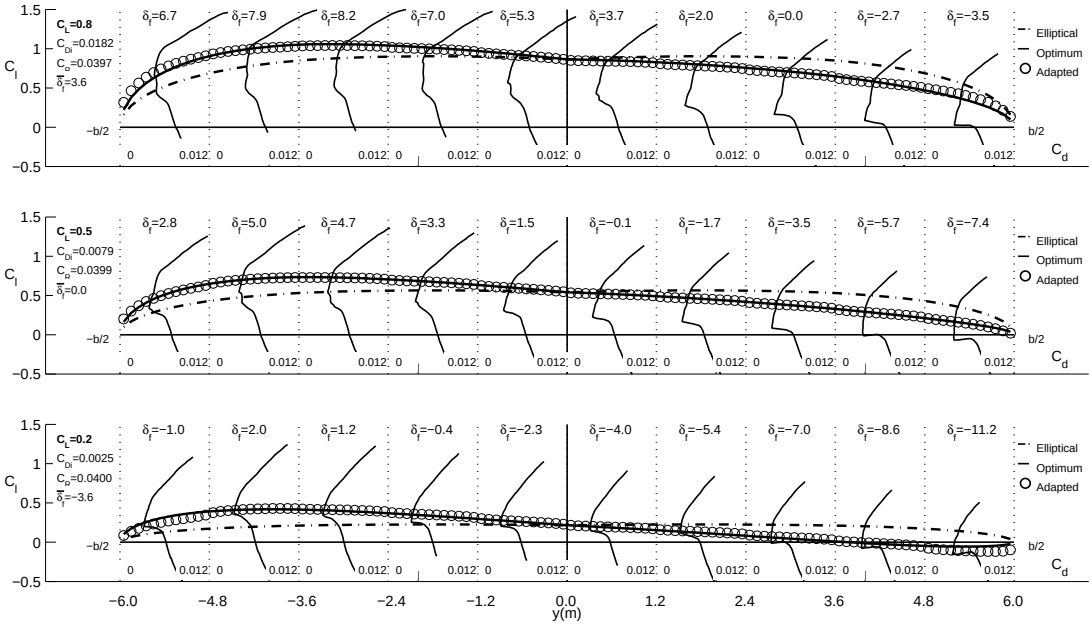

Figure 3.10: Spanwise C_l distributions with flap-section drag polars and optimal C_l distributions with $C_{R_{desired}}$=0.04 for Example Case #1 − 3.

airfoil. Even though the drag bucket is smaller both $C_{R_{desired}}$=0.02 and $C_{R_{desired}}$=0.04 cases resulted in the C_l distributions being inside the bucket. It is also found that the values of total induced drag are exact the same with the Example Case $\#1-1$ with $CAMBERED$ airfoil.

3.2.4 Example Case $\#1-4$

The last case discussed is the $REFLEXED$ airfoil used on the swept wing of $\Lambda_{c/4} = 35$ deg. Figures 3.11 and 3.12 are the C_l distributions for the $C_{R_{desired}}$=0.02 and $C_{R_{desired}}$=0.04 cases.

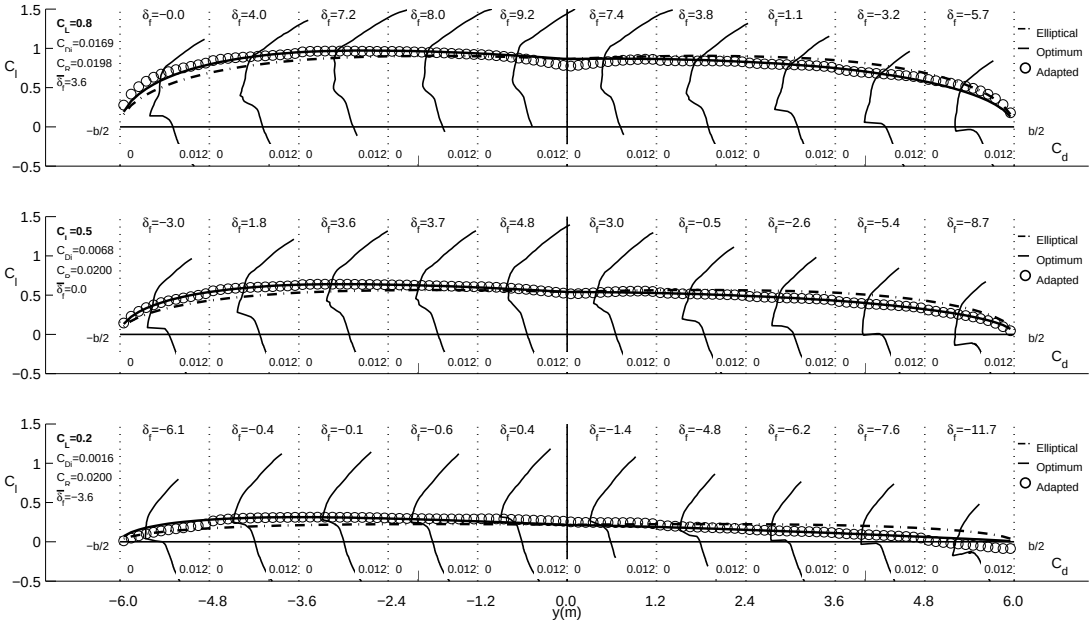

Figure 3.11: Spanwise C_l distributions with flap-section drag polars and optimal C_l distributions with $C_{R_{desired}}$=0.02 for Example Case $\#1-4$.

Comparing these two cases with the Example Case $\#1-2$, it is also found that the total induced drag for each cases are the same, which is expected because the airfoil shape does not affect the induced drag of a wing.

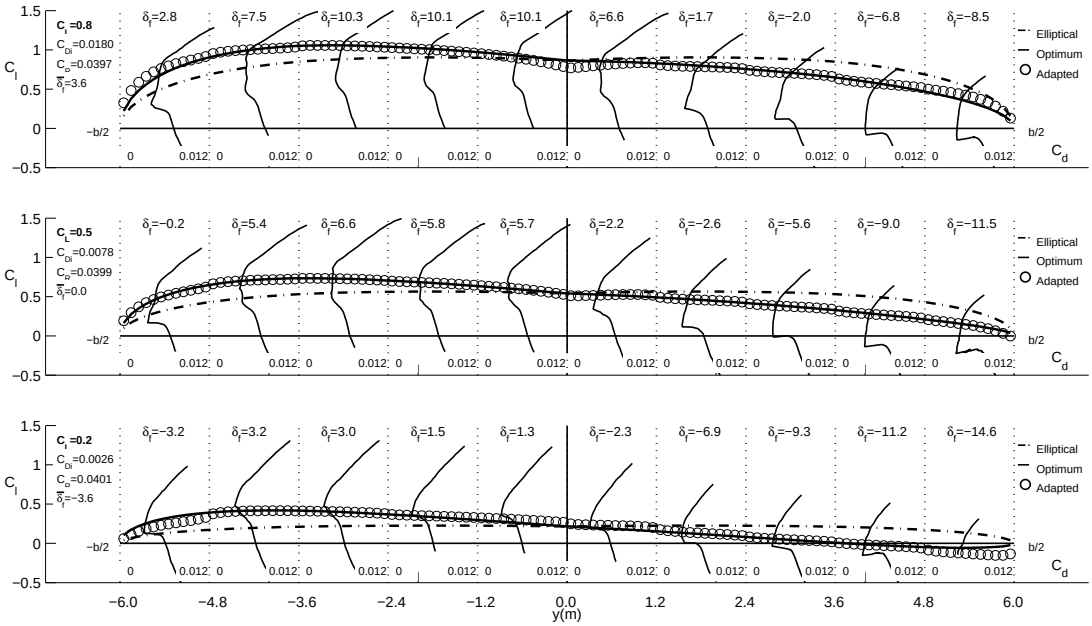

Figure 3.12: Spanwise C_l distributions with flap-section drag polars and optimal C_l distributions with $C_{R_{desired}}$=0.04 for Example Case #1 − 4.

3.2.5 Comparison of the Induced Drag

The Example Cases #1 − 1 through #1 − 4 are compared with a sample wing with ailerons. This analysis clearly shows how the theory of minimization of the induced drag was succeed.

The sample unswept wing for a comparison with the Example Cases #1 − 1 and #1 − 3 are shown in the Fig. 3.13. The sample swept wing for a comparison with the Example Cases #1−2 and #1−4 are shown in the Fig. 3.14. As shown in the planform, the two TE flaps are located at the wing tip are set as the ailerons. The same deflections are applied for both ailerons to obtain the desirable rolling moment. Then the total induced drag at the rolling moment are recorded from the AVL. Figure 3.15 through 3.18 shows the total induced drag of the wing which was compared with each corresponding example case for a range of rolling moment values.

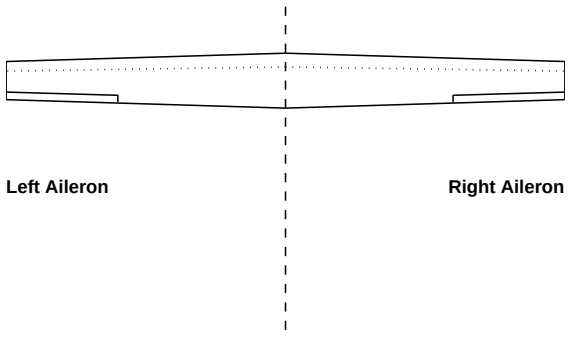

Figure 3.13: Planform of a tapered wing with ailerons.

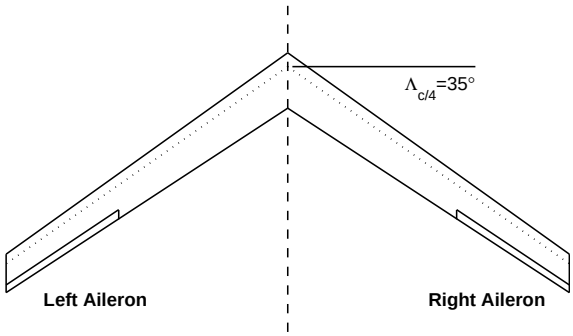

Figure 3.14: Planform of a swept wing with ailerons ($\Lambda_{c/4} = 35$).

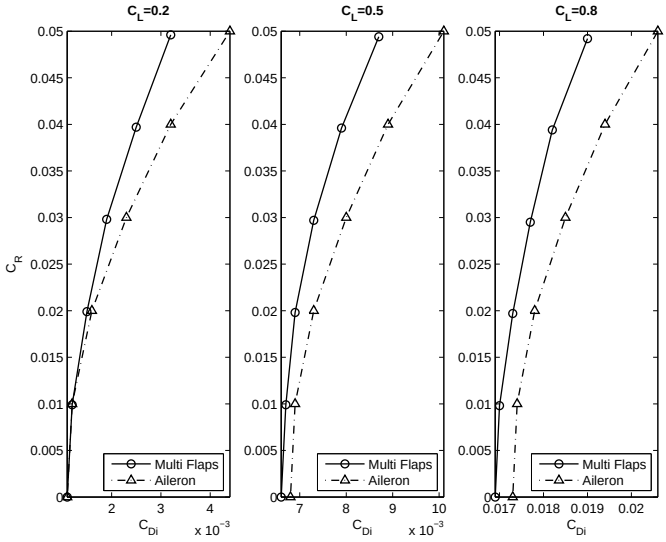

Figure 3.15: Comparison of induced drag for the unswept tapered wing with $CAMBERED$ airfoil.

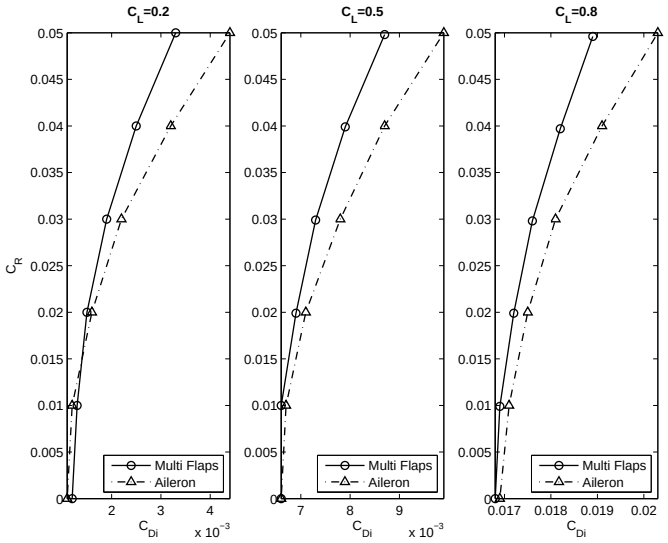

Figure 3.16: Comparison of induced drag for the unswept tapered wing with $REFLEXED$ airfoil.

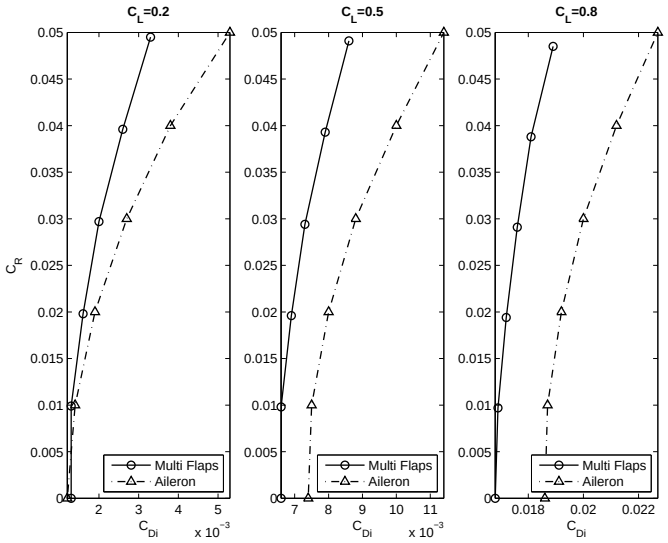

Figure 3.17: Comparison of induced drag for the swept wing with $CAMBERED$ airfoil.

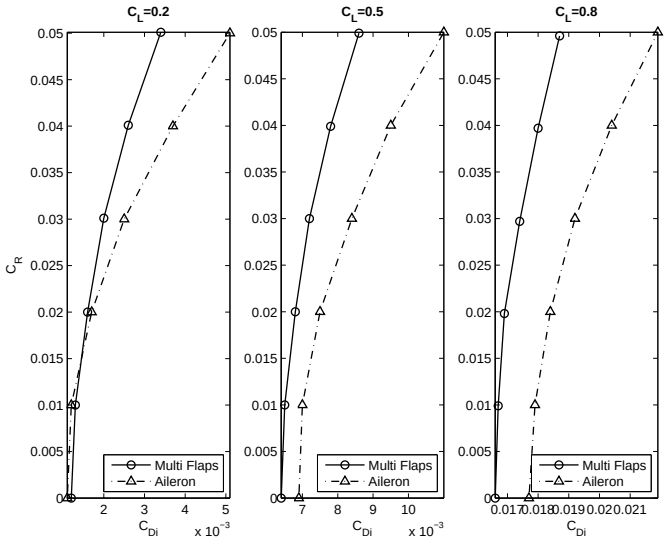

Figure 3.18: Comparison of induced drag for the swept wing with $REFLEXED$ airfoil.

These figures clearly show that the increment in the induced drag is much less for the wing with multiple TE flaps than for the wing with ailerons for all cases. Therefore, it can be concluded that the induced drag can be minimized with the desired rolling moment values using the multiple TE flaps.

3.3 Multiple Constraints of Roll and Pitch

3.3.1 Example Case $\#2-1$

In this section, several cases with the dual constraints of rolling and pitching moments are analyzed. The first case discussed is the $CAMBERED$ airfoil used on the swept wing with $\Lambda_{c/4} = 35$ deg.

Figures 3.19 and 3.20 are the C_l distributions with drag polars for $C_{R_{desired}}$ of 0.02 and 0.04 for $SchemeA$, in which there is no pitching moment constraint in determining the flaps for minimizing induced drag, and trim is achieved using the mean flap.

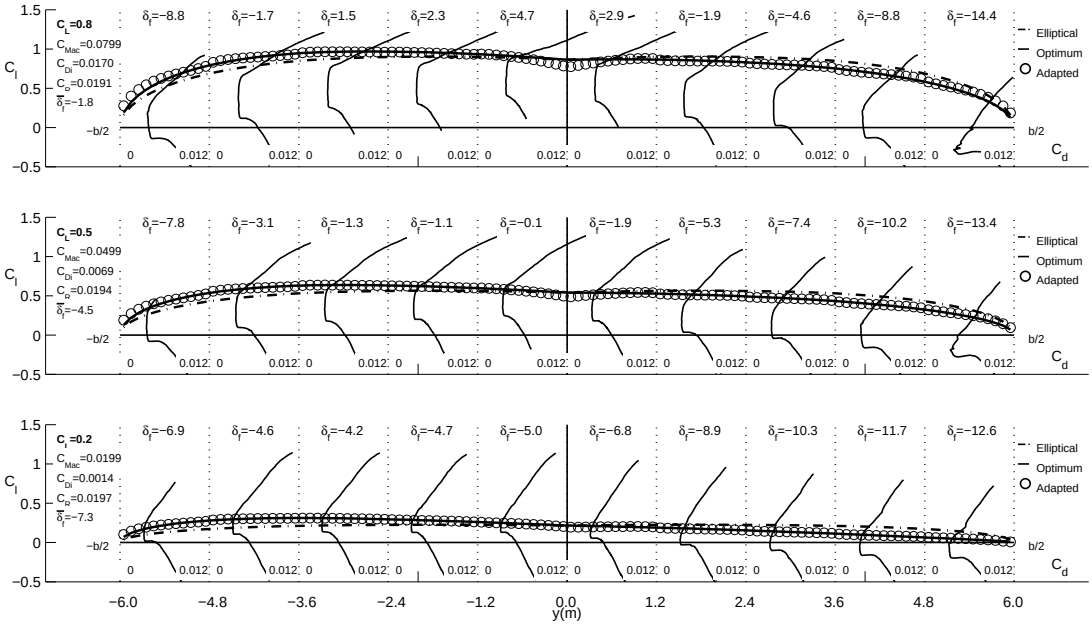

Figure 3.19: Spanwise C_l distributions with flap-section drag polars and optimal C_l distributions with $C_{R_{desired}}$=0.02 for Example Case #2 − 1, *SchemeA*.

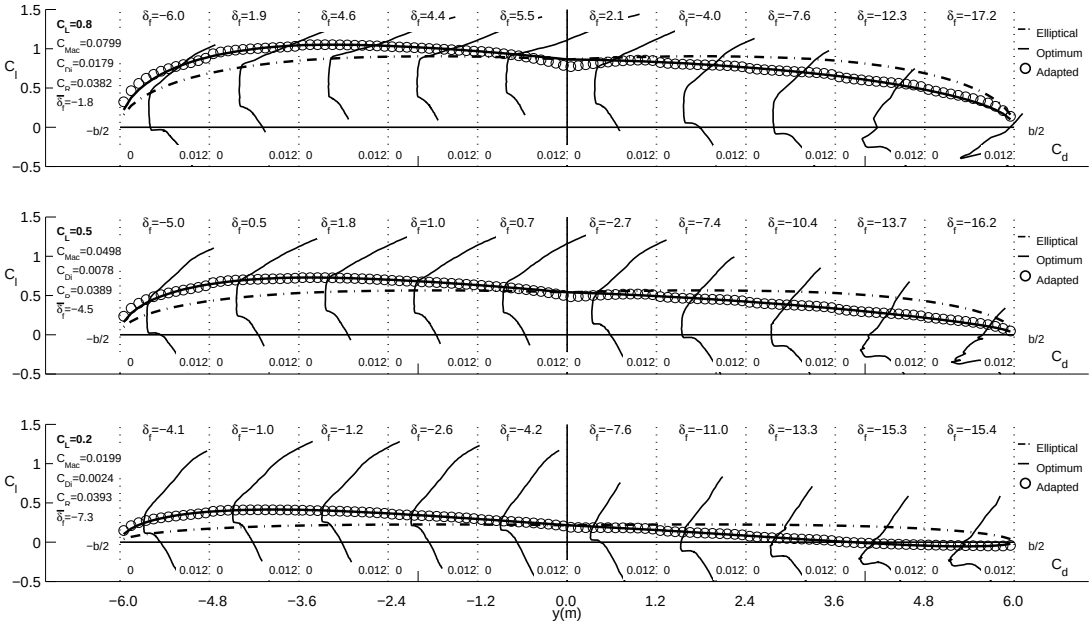

Figure 3.20: Spanwise C_l distributions with flap-section drag polars and optimal C_l distributions with $C_{R_{desired}}$=0.04 for Example Case #2 − 1, *SchemeA*.

As seen from Figures 3.19 and 3.20, at the higher C_L, the C_l distributions are not inside the drag bucket. This is because the mean flap is set for trim and not for minimizing profile drag. The desired pitching moment of the wing ($C_{M_{ac}}$) were achieved for both cases. The moment was determined by the static margin of the tailless aircraft.

Fig. 3.21 and Fig. 3.22 are the plots for the *SchemeB* for the three values of the desired rolling moment.

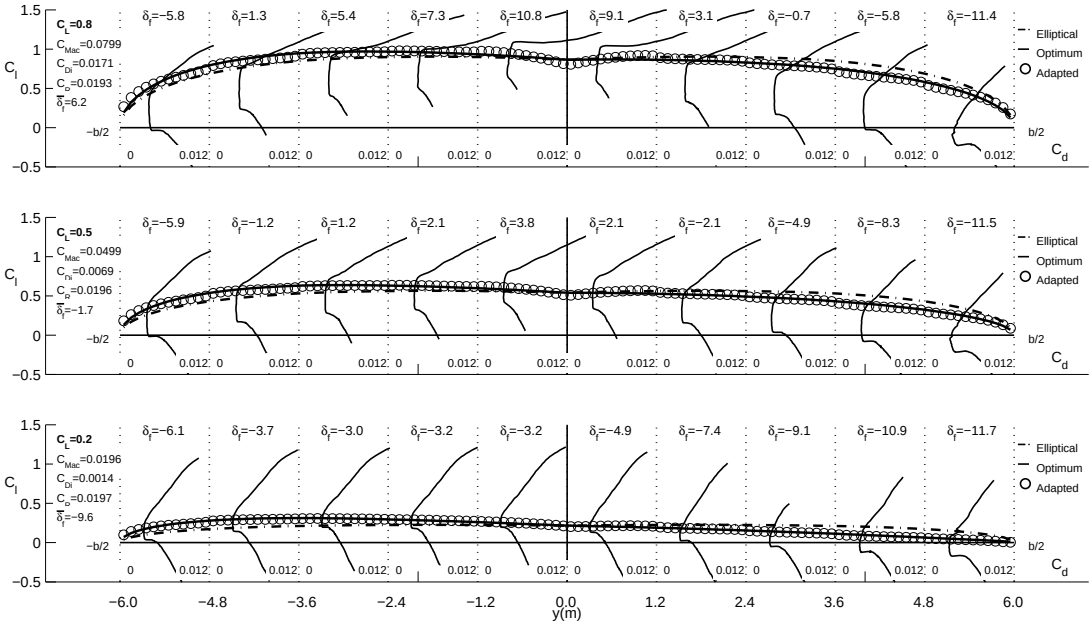

Figure 3.21: Spanwise C_l distributions with flap-section drag polars and optimal C_l distributions with $C_{R_{desired}}$=0.02 for Example Case #$2-1$, *SchemeB*.

The major difference is that the C_l distributions for *SchemeB* are inside the low drag range. This implies that the profile drag for the *SchemeB* is less than the one for *SchemeA*. This is expected phenomena because in the *SchemeB* the pitching-moment constraint is used in the minimization of induced drag and there is no effect of pitch trim in the determination of the mean flap, which is set for minimizing profile drag via drag-bucket control.

Comparison of the total induced drag between the two schemes for a range

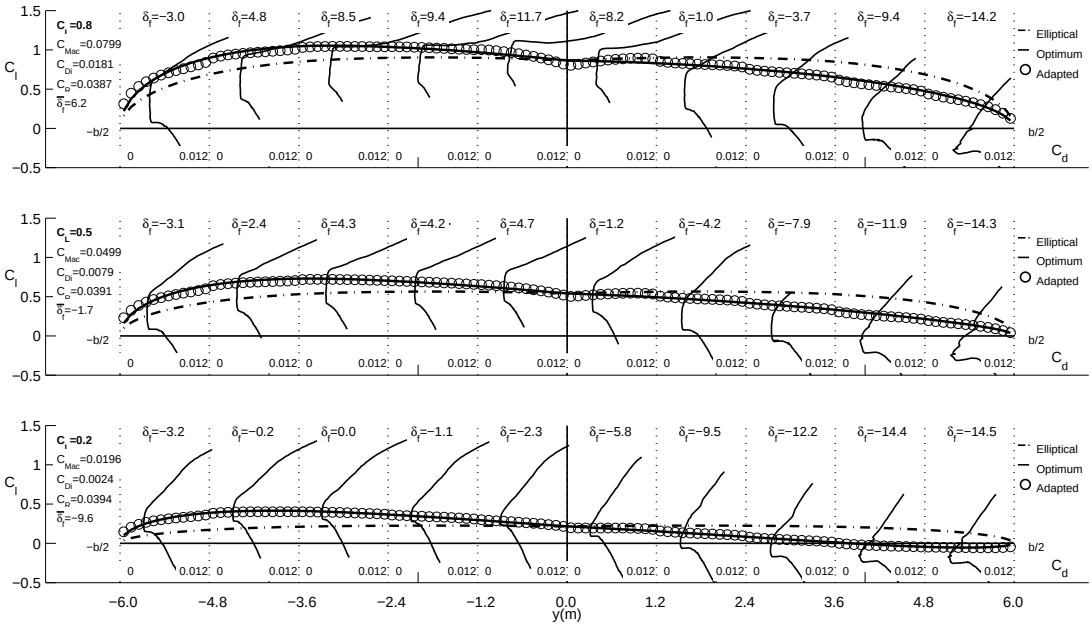

Figure 3.22: Spanwise C_l distributions with flap-section drag polars and optimal C_l distributions with $C_{R_{desired}}$=0.04 for Example Case #$2-1$, *SchemeB*.

of rolling moment is shown in Fig. 3.23. This plot shows that the induced drag values for *SchemeA* and *SchemeB* are almost the same at small C_L of 0.2, but the the difference becomes clear at the higher C_L. This is true at any values of the desired rolling moment.

3.3.2 Example Case #$2-2$

The second example case is the *REFLEXED* airfoil used on the swept wing with $\Lambda_{c/4} = 20$ deg. The reason why the *REFLEXED* airfoil was chosen for this wing because the smaller sweep angle makes it difficult to achieve the pitching moment. If the sweep angle is larger, then the moment arm for the pitching moment (distance from NP to each *a.c.* of the flap) also becomes larger. This is why the wing with $\Lambda_{c/4} = 35$ deg achieved the desired pitching moment with the *CAMBERED* airfoil. This case of wing, however, it is hard to produce the desired positive pitching moment. Therefore, the *REFLEXED* airfoil was used

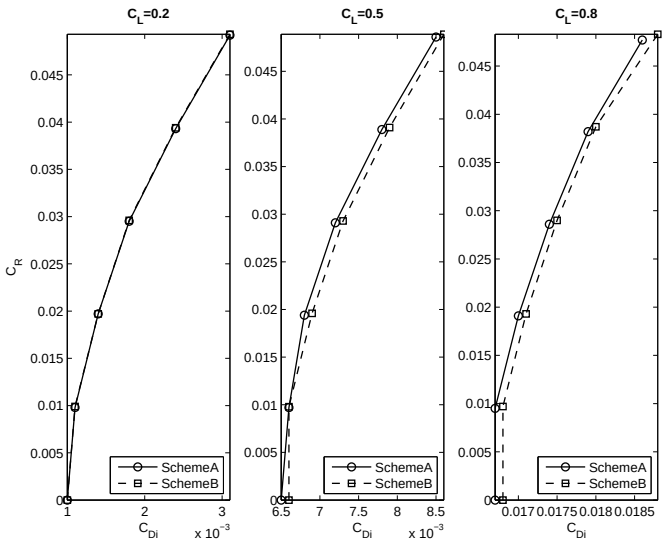

Figure 3.23: Comparison of induced drag from $SchemeA$ and $SchemeB$.

so that the airfoil itself can produce the positive pitching moment to help achieve the desired moment on the wing.

Figures 3.24 and 3.25 are the C_l distributions with the drag polars for $SchemeA$ at each desired rolling moment.

Since this is $SchemeA$ some of the C_l distributions are not inside the drag bucket. For example, at $C_L = 0.2$, all the flaps did not result in the minimum profile drag. This is again because the $SchemeA$ was the minimization of the induced drag only. However, the desired pitching moment at the N.P. was obtained, just like the Example Case $\#2 - 1$. Therefore, the tailless aircraft with this adaptive flap deflections can be trimmed.

For $SchemeB$, the following plots in the Figures 3.26 and 3.27 show the C_l distributions with drag polars for the two desired rolling moment values.

It is found that all the C_l distributions are obtained inside the low drag range. At $C_L = 0.2$, flaps located near the root required large amount of negative deflections. This is because the airfoil needs to generate the desirable pitching moment as well as enable operation of the section inside the drag bucket. Total induced

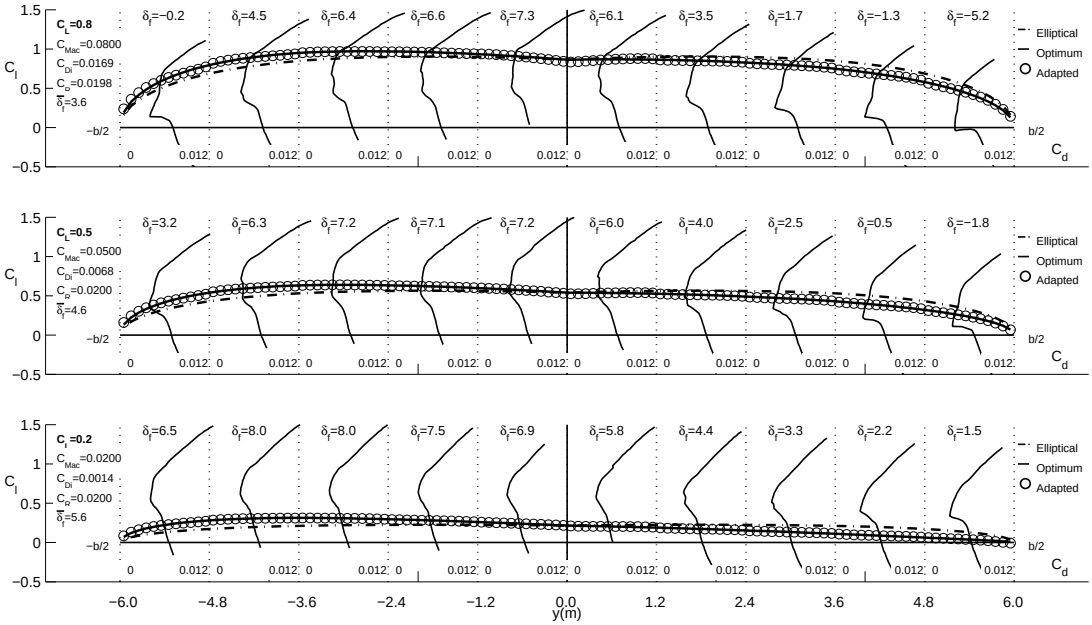

Figure 3.24: Spanwise C_l distributions with flap-section drag polars and optimal C_l distributions with $C_{R_{desired}}$=0.02 for Example Case #2 − 2, *SchemeA*.

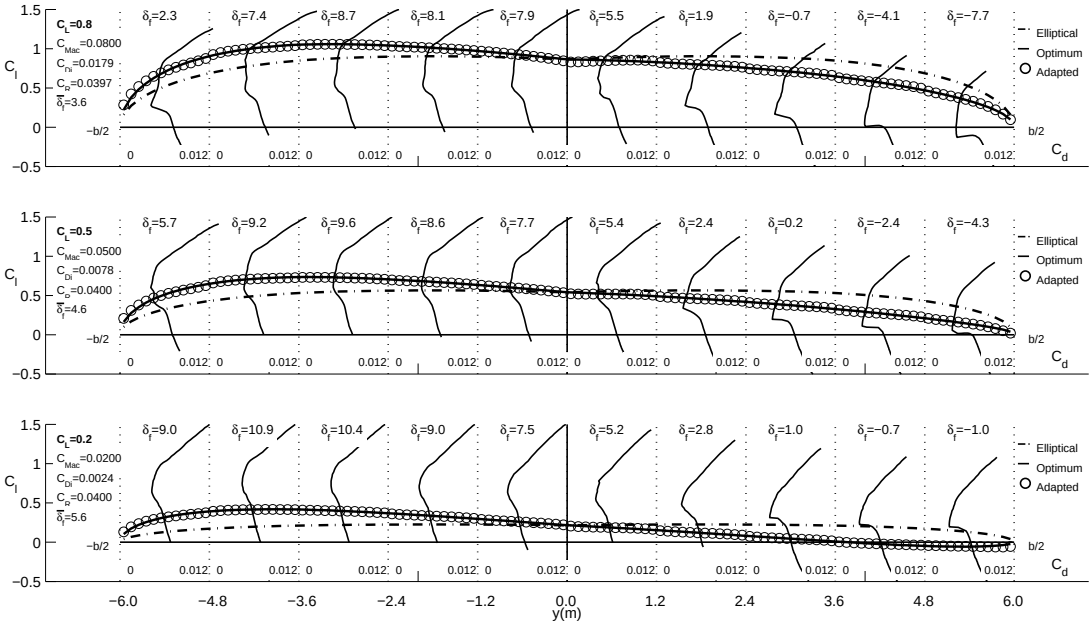

Figure 3.25: Spanwise C_l distributions with flap-section drag polars and optimal C_l distributions with $C_{R_{desired}}$=0.04 for Example Case #2 − 2, *SchemeA*.

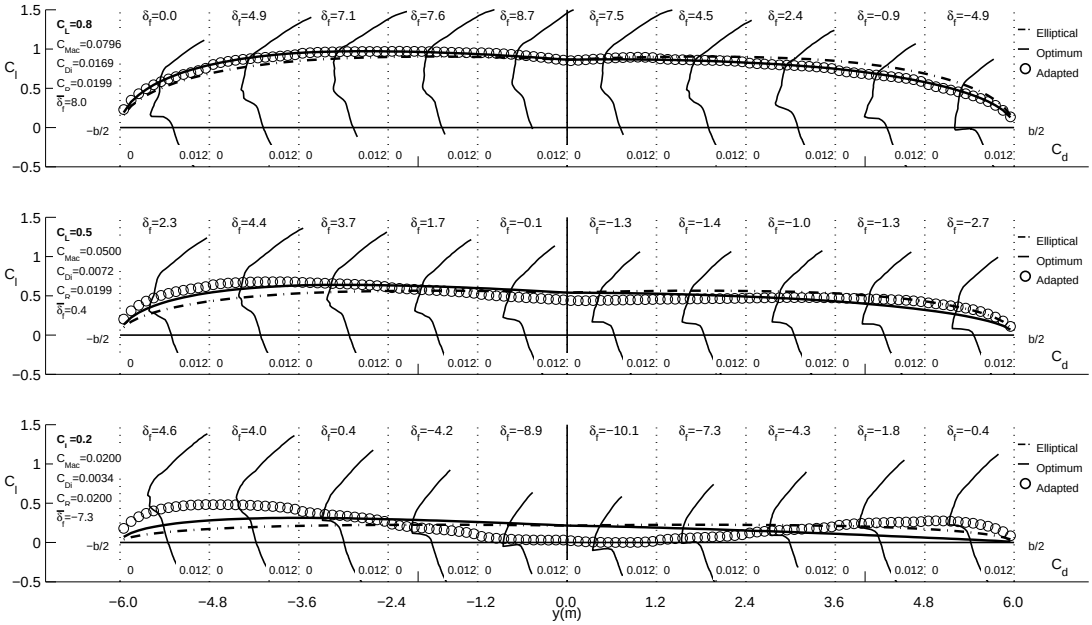

Figure 3.26: Spanwise C_l distributions with flap-section drag polars and optimal C_l distributions with $C_{R_{desired}}$=0.02 for Example Case #2 − 2, *SchemeB*.

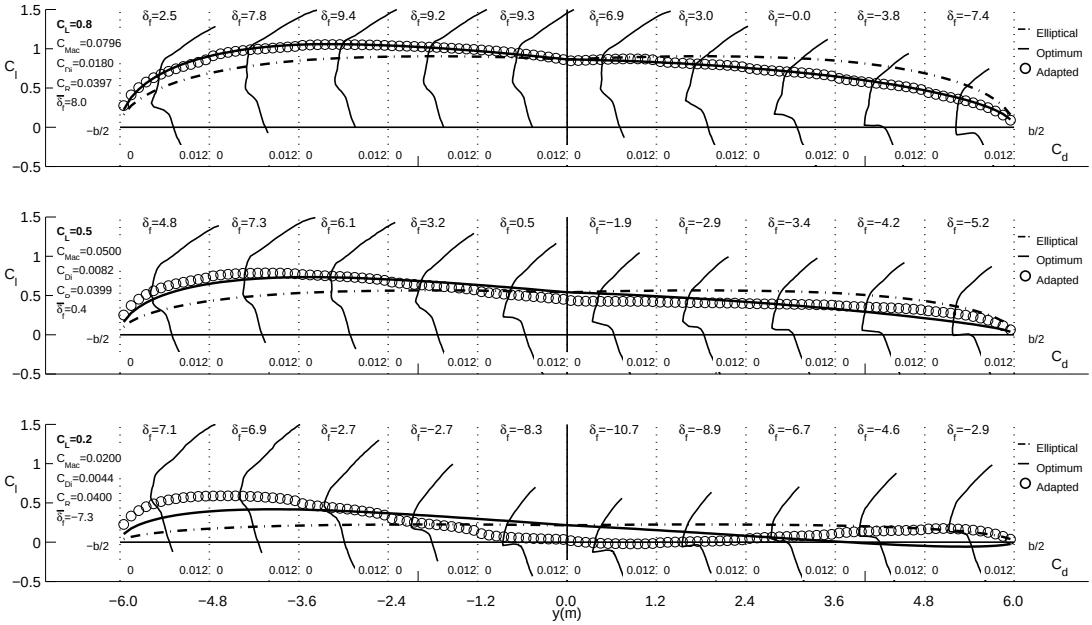

Figure 3.27: Spanwise C_l distributions with flap-section drag polars and optimal C_l distributions with $C_{R_{desired}}$=0.04 for Example Case #2 − 2, *SchemeB*.

drag of this wing for both schemes are analyzed for a range of rolling moment in the Fig. 3.28.

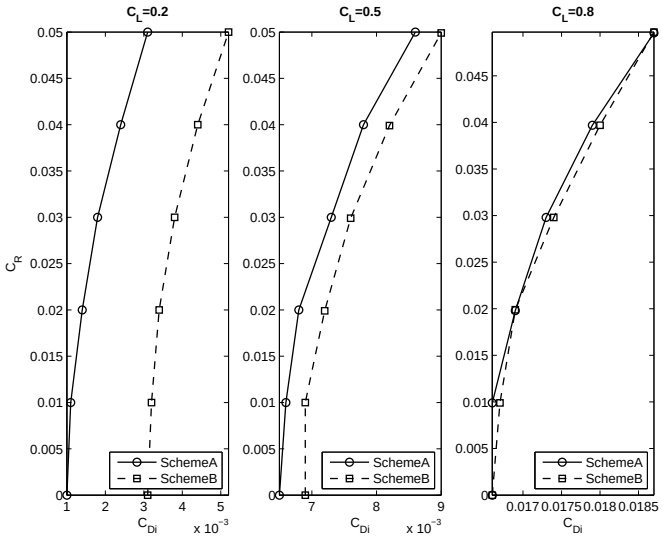

Figure 3.28: Comparison of induced drag from $SchemeA$ and $SchemeB$.

As it can be seen in the plot, there are significant differences in the induced drag between the two schemes at $C_L = 0.2$. This is already found from the Figures 3.26 and 3.27 that the C_l distributions at this wing C_L is way off from the optimum distributions. This is only at the low wing C_L. Once the wing C_L increases, the amount of the induced drag from the two schemes are closer.

3.3.3 Comparison of the Induced Drag

The Example Cases $\#2-1$ and $\#2-2$ are compared with a sample wing with ailerons. This analysis clearly shows how the theory of minimization of the induced drag is successful.

The sample wing for a comparison with the Example Cases $\#2-1$ is shown in the Fig. 3.14. It is the same sweep angle of $\Lambda_{c/4} = 35$ deg with the $CAMBERED$ airfoil. As shown in the planform, the two TE flaps located at the wing tip are set as the ailerons. The same deflections are applied for both ailerons to obtain

the desirable rolling moment. Then the total induced drag is obtained from the AVL. Figure 3.29 shows the total induced drag of the wing which was compared with the Example Case $\#2-1$ for a range of rolling moment.

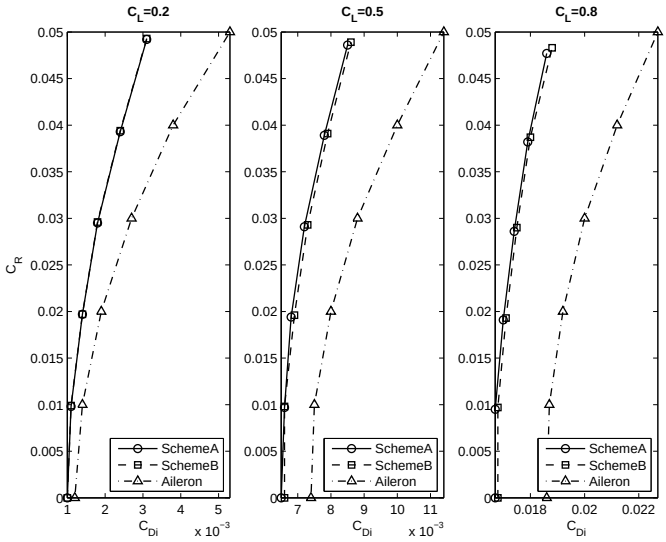

Figure 3.29: Comparison of induced drag from *SchemeA* and *SchemeB* and a wing with ailerons.

The Figure 3.29 clearly shows how the total induced drag is reduced when using multiple TE flaps. The rate of increment is obviously larger on the wing with ailerons. At $C_L = 0.2$ the induced drag for both *SchemeA* and *SchemeB* are approximately the half of the value on the sample wing. This results showed that the minimization of the total induced drag with the rolling and pitching moment constraints are successfully achieved for the Example Case $\#2-1$.

The sample wing for a comparison with the Example Cases $\#2-2$ is shown in the Figure 3.30. It is the same sweep angle of $\Lambda_{c/4} = 20$ deg with the $REFLEXED$ airfoil. The aileron sizing is the same with the previous sample wing. The comparison of the total induced drag is shown in the Figure 3.31.

The Figure 3.31 shows that the induced drag is higher on *SchemeB* than the sample wing with ailerons at $C_L = 0.2$. However, when the C_L increases, the *SchemeB* achieves less induced drag than the aileron case. The *SchemeA* achieves

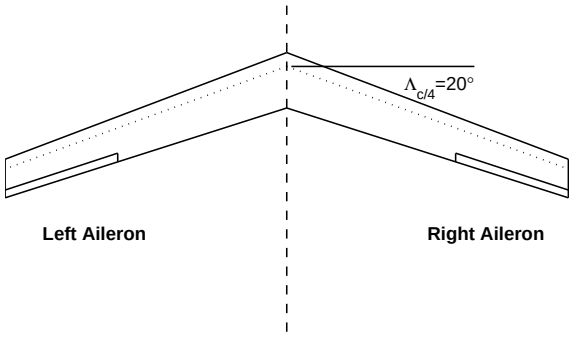

Figure 3.30: Planform of a swept wing with ailerons ($\Lambda_{c/4} = 20$).

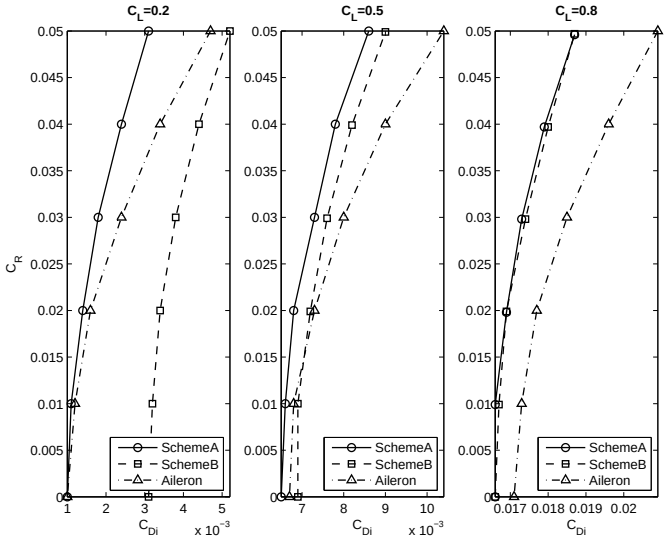

Figure 3.31: Comparison of induced drag from *SchemeA* and *SchemeB* and a wing with ailerons.

the lowest induced drag because it is not under the consideration of minimization of profile drag.

3.4 Adapted Distribution Due to a Stuck Flap

The results for control failure leading to a stuck flap are shown in this section. The Figures 3.32, 3.33, and 3.34 are the C_l distributions with different desired rolling moment when the $Flap1$ (a flap on the left wing tip) is stuck at zero degree of deflection.

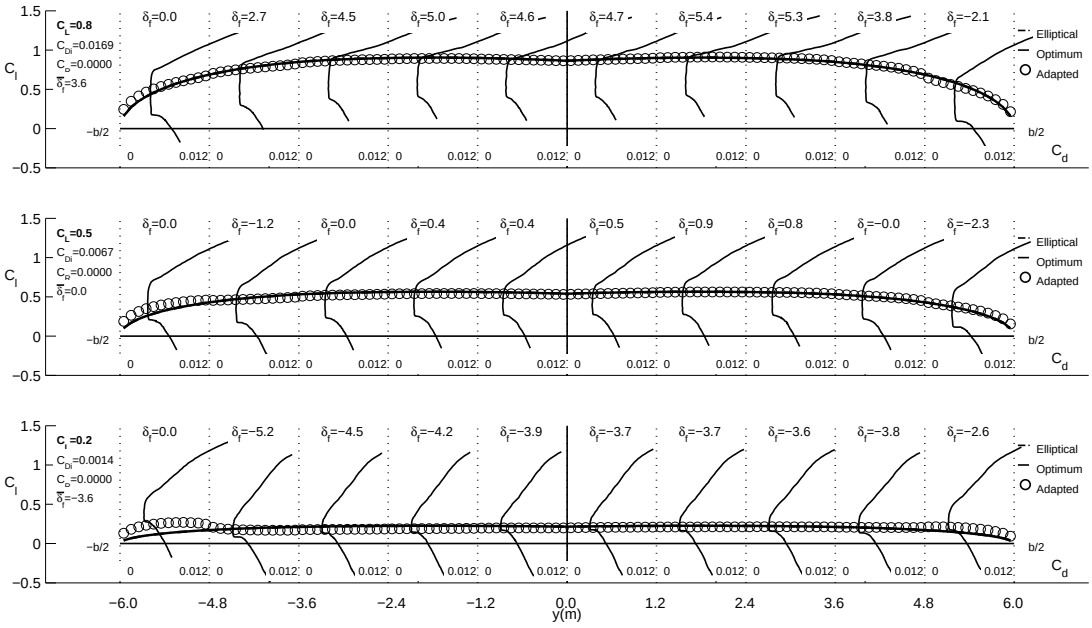

Figure 3.32: Spanwise C_l distributions with flap-section drag polars and optimal C_l distributions with $C_{R_{desired}}$=0.00 when $Flap1$ is stuck with zero deflection.

The results clearly show that the adaptive flaps are still able to obtain the desired rolling moment when the $Flap1$ is stuck with zero deflection. Obviously this is because the stuck deflection of zero is very close to the actual adaptive deflection. This is why the C_l distribution at this flap location is inside the drag bucket.

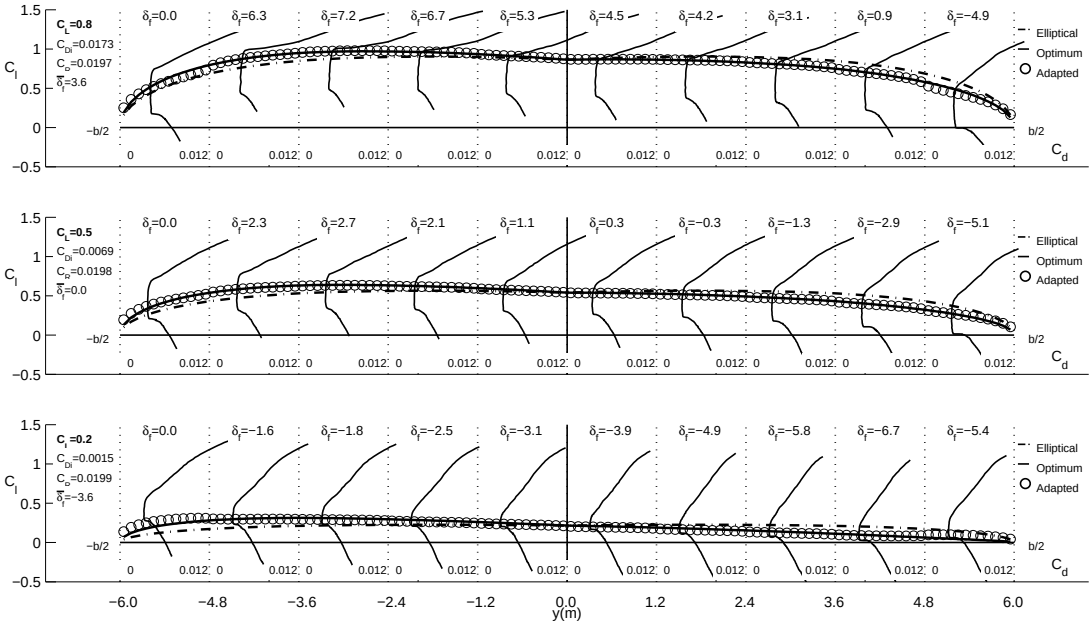

Figure 3.33: Spanwise C_l distributions with flap-section drag polars and optimal C_l distributions with $C_{R_{desired}}$=0.02 when $Flap1$ is stuck with zero deflection.

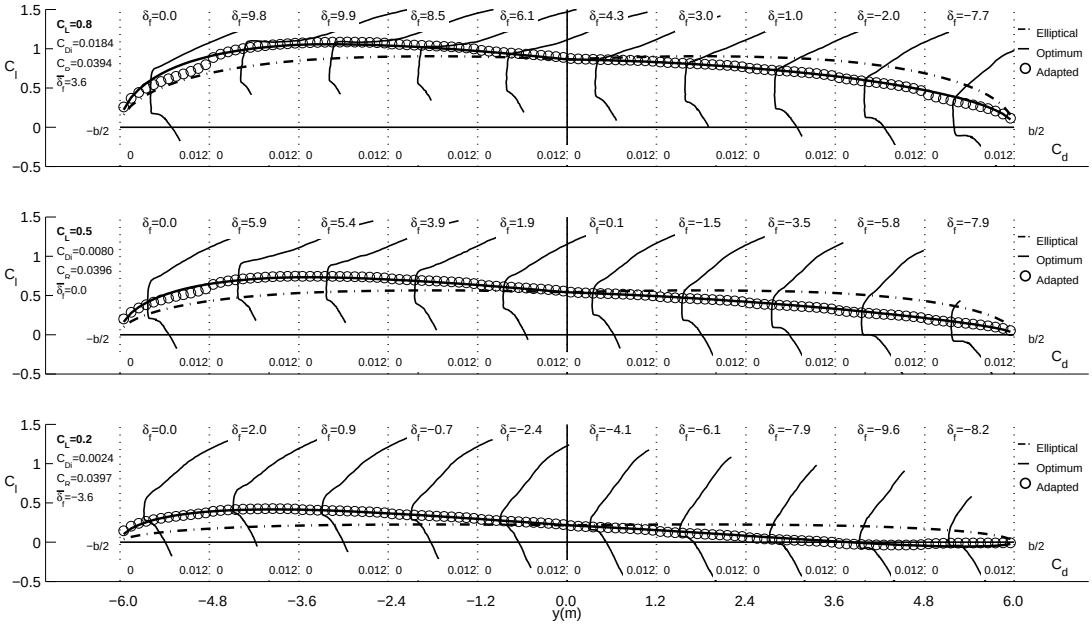

Figure 3.34: Spanwise C_l distributions with flap-section drag polars and optimal C_l distributions with $C_{R_{desired}}$=0.04 when $Flap1$ is stuck with zero deflection.

The next following plots in Figures 3.35, 3.36, and 3.37 are cases when the $Flap1$ was stuck with 10 degrees of deflection.

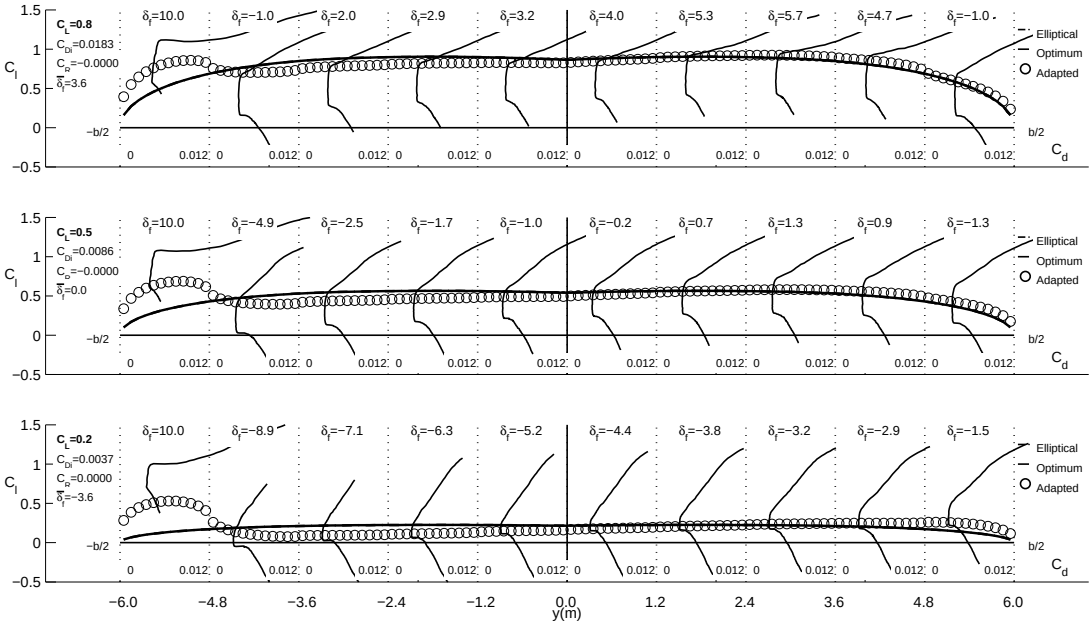

Figure 3.35: Spanwise C_l distributions with flap-section drag polars and optimal C_l distributions with $C_{R_{desired}}$=0.00 when $Flap1$ is stuck at δ_f=10 deg.

As it can be seen in the plots, it was hard to obtain the drag polar at the stuck flap of $Flap1$ since the flap deflection was too large. Because of this there would be a large amount of profile drag due to the separation. However, the desired rolling moment was also achieved with the reduced induced drag. This implies that the adaptive flaps are still able to achieve the desired rolling moment when the stuck flap has a large deflection angle.

Figures 3.38, 3.39, and 3.40 are the C_l distributions when the $Flap6$ (a flap on right hand side next to the root) was stuck with zero deflection.

Since the deflection is zero, drag polars for the stuck flap were easily obtained. At the $C_L = 0.5$, the zero deflection seemed the appropriate adaptive flap deflection. Even for cases with $C_L = 0.2$ and $C_L = 0.8$, the stuck flap did not affect much to the contribution of generating optimum distribution. Therefore,

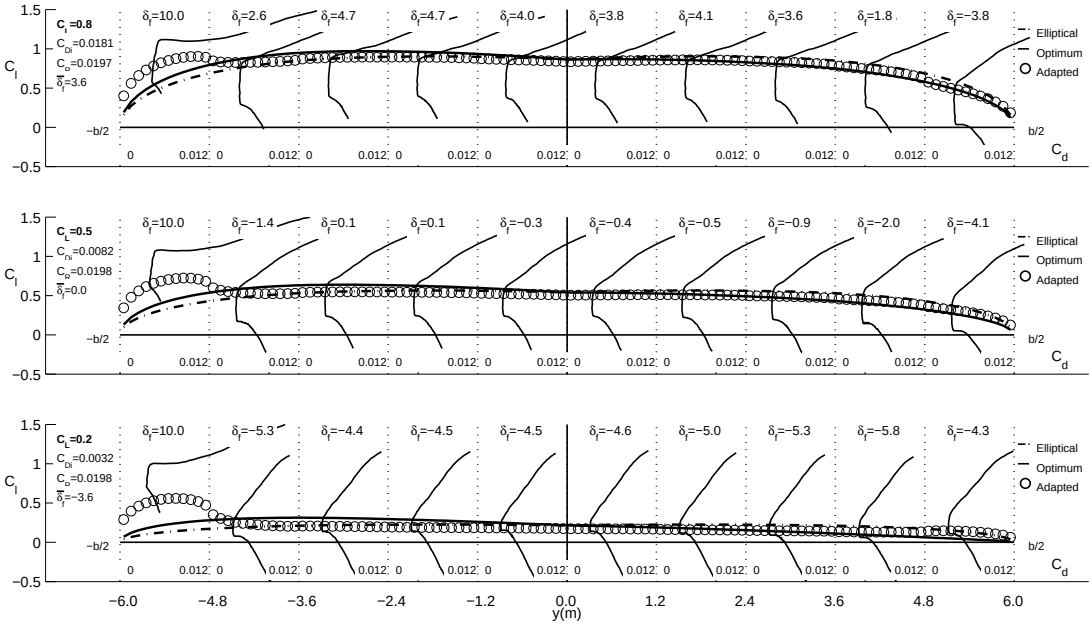

Figure 3.36: Spanwise C_l distributions with flap-section drag polars and optimal C_l distributions with $C_{R_{desired}}$=0.02 when $Flap1$ is stuck at δ_f=10 deg.

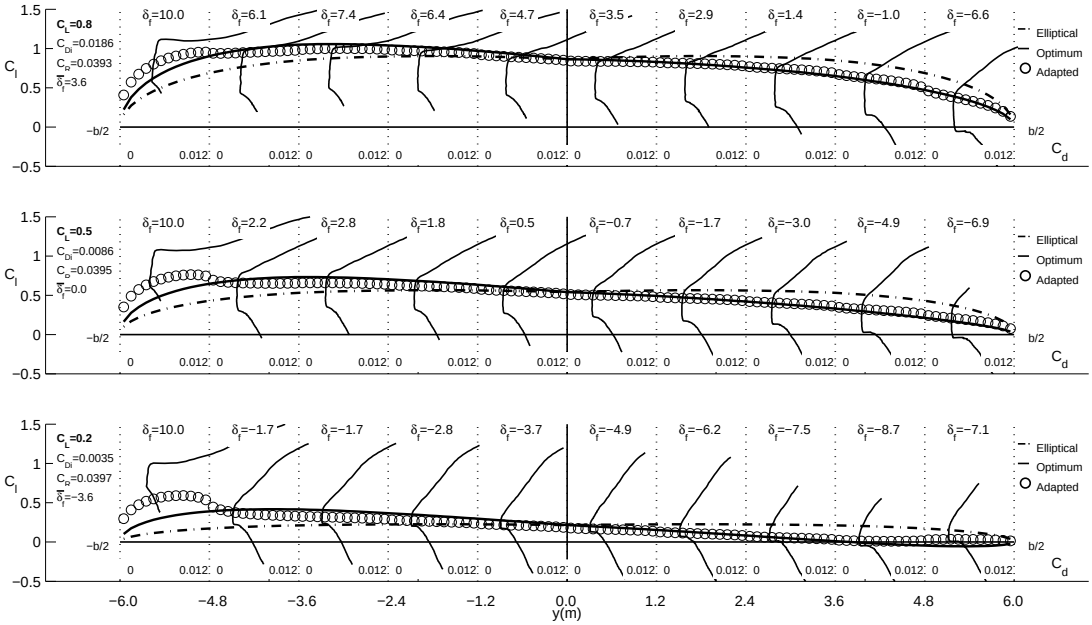

Figure 3.37: Spanwise C_l distributions with flap-section drag polars and optimal C_l distributions with $C_{R_{desired}}$=0.04 when $Flap1$ is stuck at δ_f=10 deg.

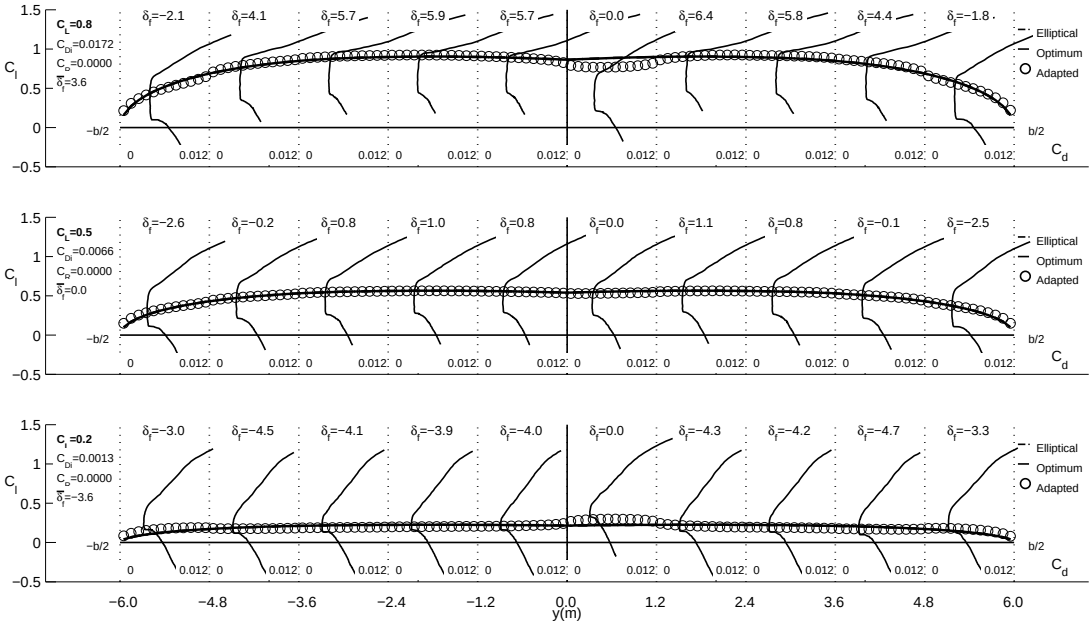

Figure 3.38: Spanwise C_l distributions with flap-section drag polars and optimal C_l distributions with $C_{R_{desired}}$=0.00 when $Flap6$ is stuck with zero deflection.

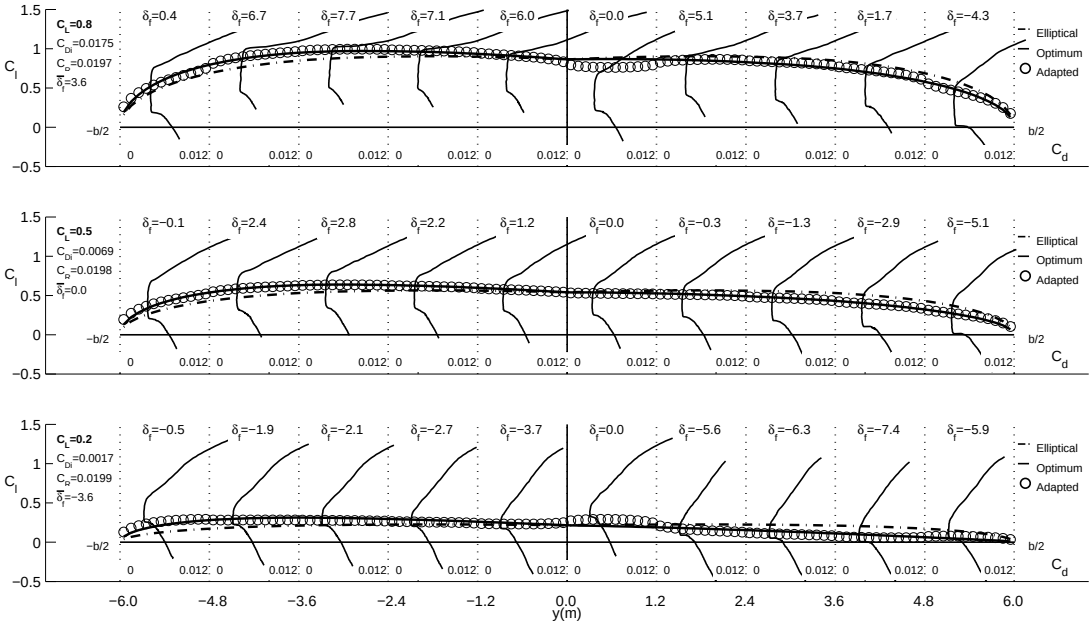

Figure 3.39: Spanwise C_l distributions with flap-section drag polars and optimal C_l distributions with $C_{R_{desired}}$=0.02 when $Flap6$ is stuck with zero deflection.

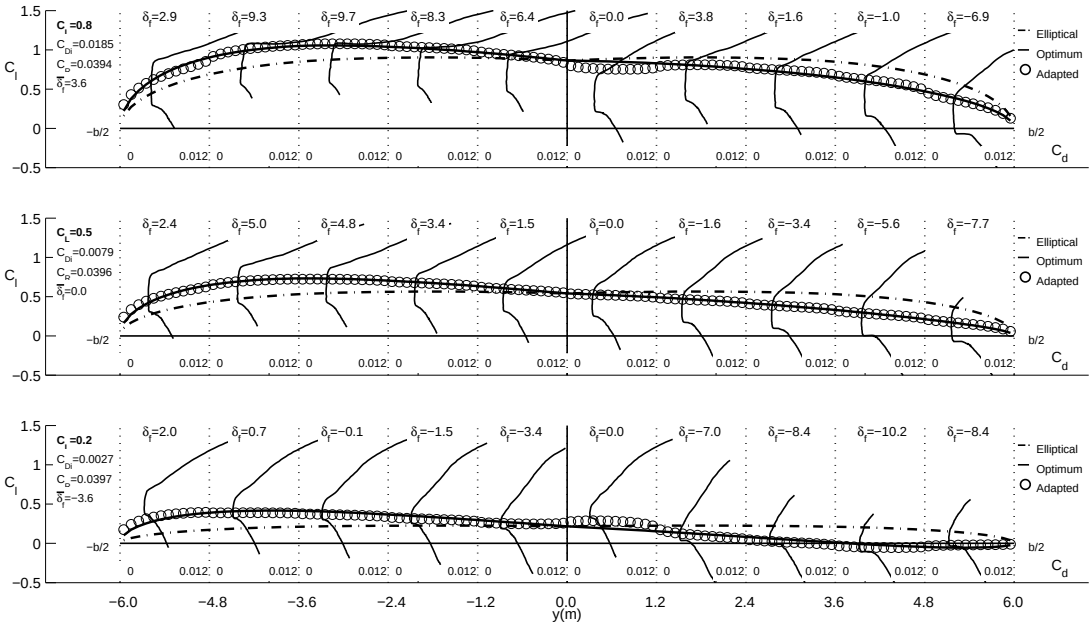

Figure 3.40: Spanwise C_l distributions with flap-section drag polars and optimal C_l distributions with $C_{R_{desired}}$=0.04 when $Flap6$ is stuck with zero deflection.

the adaptive flaps achieved the desired rolling moment with reduced induced drag when the $Flap6$ were stuck with zero deflection.

The next plots of Figures 3.41, 3.42, and 3.43 are the cases of the stuck flap with 10 degrees of deflection.

For this case also, it is difficult to obtain the drag polar for the stuck flap, because the flap deflection is too large. However, the desired rolling moment was obtained.

From these results shown in this section, it can be concluded that the adaptive flaps are able to achieve its desirable rolling moment even though one of the flaps is stuck at some deflection angle. If the deflection angle of the stuck flap were large, then the wing would not be able to generate an attached flow around the stuck flap. However, the rest of the controllable flaps can adjust to achieve the rolling moment control.

This section only showed the single constraint of rolling moment, but the

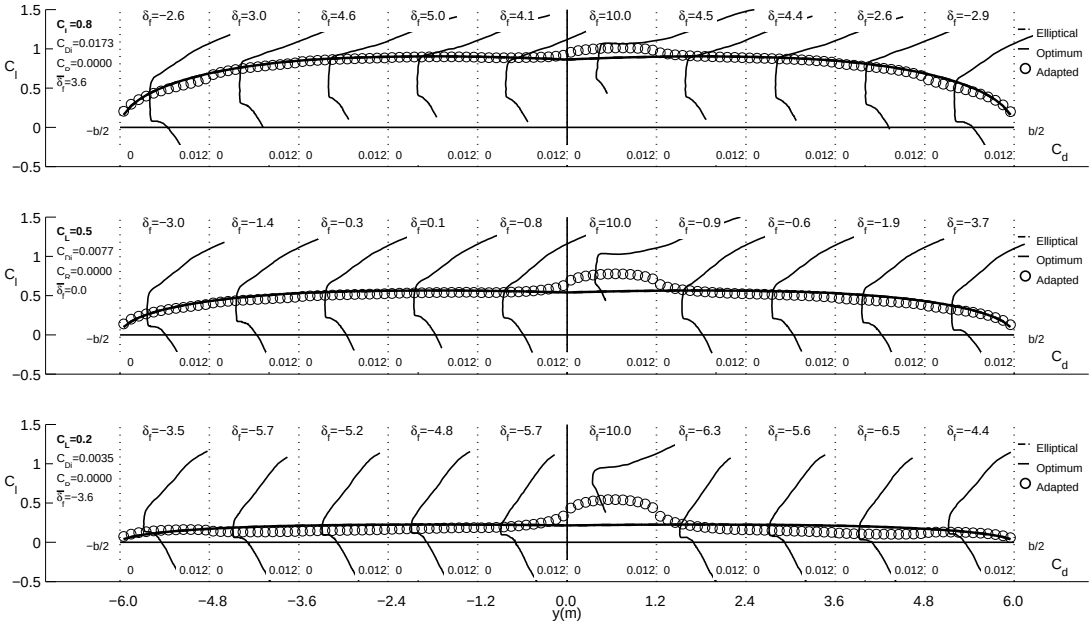

Figure 3.41: Spanwise C_l distributions with flap-section drag polars and optimal C_l distributions with $C_{R_{desired}}$=0.00 when $Flap6$ is stuck at δ_f=10 deg.

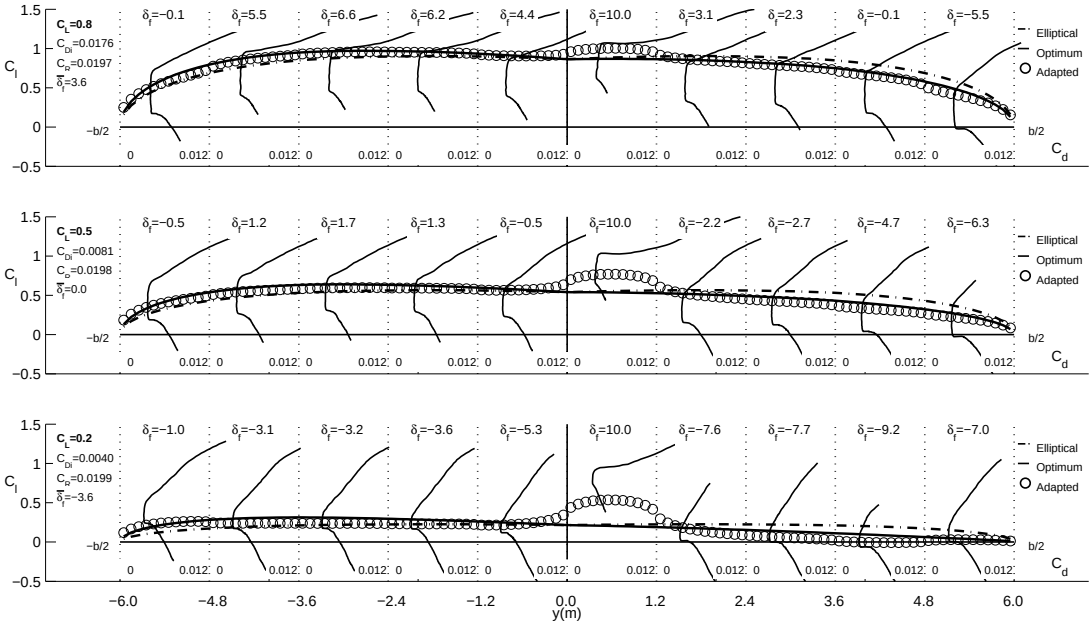

Figure 3.42: Spanwise C_l distributions with flap-section drag polars and optimal C_l distributions with $C_{R_{desired}}$=0.02 when $Flap6$ is stuck at δ_f=10 deg.

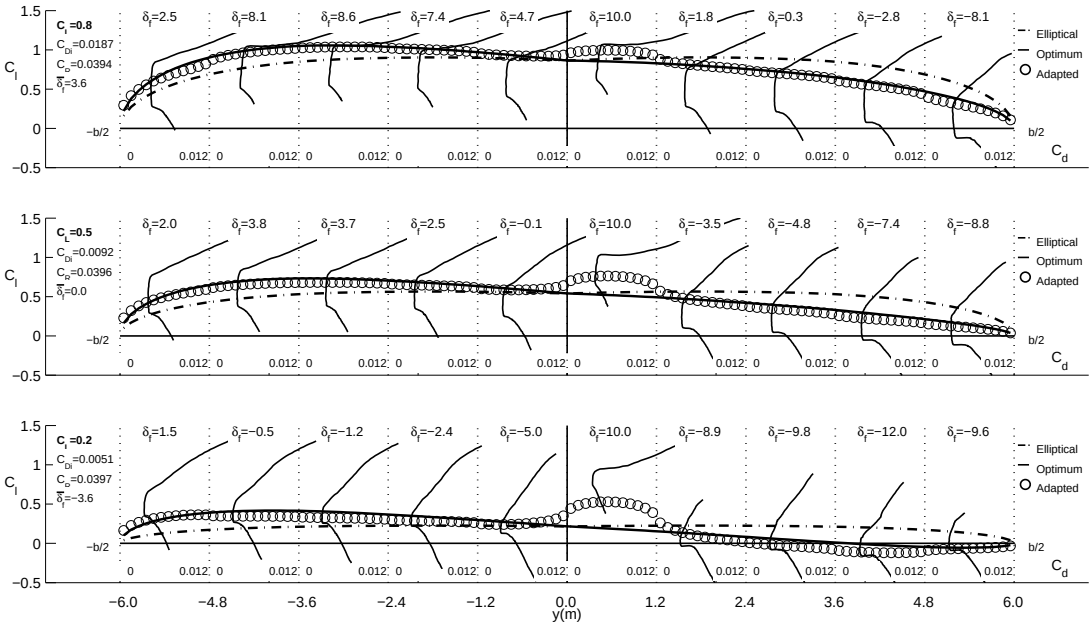

Figure 3.43: Spanwise C_l distributions with flap-section drag polars and optimal C_l distributions with $C_{R_{desired}}$=0.04 when $Flap6$ is stuck at δ_f=10 deg.

theory also can be applied for two constraints of the roll and the pitching moment. In other words, the tailless aircraft with the multiple TE flaps would also be able to satisfy the constraints in the event of a control failure. More than that, this theory can be extended for a case with multiple flaps were stuck. Obviously it is expected that if the number of stuck flaps increased then it would be difficult for a wing to achieve the desirable moment control. However, if only a small number of flaps have control failures, then the remaining flaps will be able to provide the required redundancy.

Chapter 4

Concluding Remarks

Building on recent research efforts in the use of multiple trailing-edge flaps on aircraft wings, the current research explores the use of these flaps for efficiently generating rolling moments. By decomposing the spanwise loading using the concept of basic and additional lift distributions and by using the theory of relative extrema, a methodology was developed for determining the optimum flap angles for minimizing drag at a specified lift coefficient while generating the desired rolling moment. The system matrices needed for the solutions can be pre-computed and stored. The computations involve solutions of simple matrix equations, which can be easily accomplished even on a flight computer. The methodology has also been applied to roll control on a tailless aircraft, in which the rolling moment has been applied as a second constraint in addition to the pitching-moment constraint. The results show that generating rolling moments using the optimum flap angles often results in significantly less induced drag than when using ailerons.

For most aircraft and most missions, the fraction of the flight time during which rolling moments are required is very small. For this reason, the reduction in drag achieved when generating a rolling moment with multiple TE flaps is unlikely to result in significant improvements in performance or fuel burn of transport aircraft. The current work may, however, provide strategies for noticeable performance improvement on sailplanes and other aircraft for which turning

flight and rolling into and out of turns is a considerable fraction of the flight duration. The current work also serves as a stepping stone to studying the benefits of distributed effectors for efficient aircraft control. Furthermore, the redundancy provided by the multiple flaps may prove beneficial in the event of control failures. As an exploration of such benefits, the current methodology was used to study the situation in which one or more flaps are stuck at some angle due to failure. The results provide confidence that the controllable flaps are able to compensate for the stuck flaps. This exploratory work suggests that the topic is worth further investigation in a follow-on research effort. Additionally, it is possible that the use of multiple flaps may provide the capability to generate rolling moment with minimum adverse yaw, leading to improvements in airplane handling. It is, therefore, recommended that the current study be extended to explore the adverse yaw minimization with multiple flaps.

Chapter 5

References

[1] Lilienthal, O., *Birdflight As The Basis Of Aviation*, American Aeronautical Archives, 2nd ed., 2001.

[2] Raymer, D. P., *Aircraft Design: A Conceptual Approach*, American Institute of Aeronautics and Astronautics, Inc., 3rd ed., 1999.

[3] Pfenninger, W., "Investigation on Reductions of Friction on Wings, in Particular by Means of Boundary Layer Suction," NACA TM 1181, August 1947.

[4] Pfenninger, W., "Experiments on a Laminar Suction Airfoil of 17 Per Cent Thickness," *Journal of the Aeronautical Sciences*, April 1949, pp. 227–236.

[5] McGhee, R. J., Viken, J. K., Pfenninger, W., Beasley, W. D., and Harvey, W. D., "Experimental Results for a Flapped Natural-Laminar-Flow Airfoil with High Lift/Drag Ratio," NASA TM 85788, May 1984.

[6] Viken, J. K., "Boundary-Layer Stability and Airfoil Design," *Laminar Flow Aircraft Certification*, NASA CP 2413, 1985, pp. 1–30.

[7] Somers, D. M., "Design and Experimental Results for a Flapped Natural-Laminar-Flow Airfoil for General Aviation Applications," NASA TP 1865, June 1981.

[8] Viken, J. K., *Aerodynamic Design Considerations and Theoretical Results for a High Reynolds Number Natural Laminar Airfoil*, Master's thesis, George Washington University, 1983.

[9] Drela, M., "Elements of Airfoil Design Methodology," *Applied Computational Aerodynamics*, edited by P. A. Henne, Vol. 125, AIAA, Washington, DC, 1990, pp. 167–189.

[10] Althaus, D., *Niedrig-geschwindigkeits-profile*, Friedr. Vieweg & Sohn Verlagsgesellschaft mbH, Braunschweig/Wiesbaden, 1996.

[11] McAvoy, C. W. and Gopalarathnam, A., "Automated Cruise Flap for Airfoil Drag Reduction Over a Large Lift Range," *Journal of Aircraft*, Vol. 39, No. 6, November–December 2002, pp. 981–988.

[12] Stanewsky, E., "Aerodynamic benefits of adaptive wing technology," *Aerospace Science and Technology*, Vol. 4, 2000, pp. 439–452.

[13] Spillman, J. J., "The use of variable camber to reduce drag, weight and costs of transport aircraft," *Aeronautical Journal*, 1992.

[14] McAvoy, C. W. and Gopalarathnam, A., "Automated Trailing-Edge Flap for Airfoil Drag Reduction Over a Large Lift-Coefficient Range," AIAA Paper 2002–2927, June 2002.

[15] Jepson, J. K., *Advancements in Aerodynamic Technologies for Airfoils and Wings*, Ph.D. thesis, North Carolina State University, Raleigh, North Carolina, December 2006.

[16] King, R. M. and Gopalarathnam, A., "Ideal Lift Distributions and Flaps Angles for Adaptive Wings," AIAA Paper 2004–4722, August 2004.

[17] Cusher, A. A. and Gopalarathnam, A., "Drag Reduction Methodology for Adaptive Tailless Aircraft," AIAA Paper 2006–3320, June 2006.

[18] Azuma, A., *The Biokinetics of Flying and Swimming*, American Institute of Aeronautics and Astronautics, Inc., 2nd ed., 2006.

[19] Bryson, A. E. and Ho, Y.-C., *Applied Optimal Control*, John Wiley and Sons, Inc., 1975.

[20] Anderson, J. D., *Fundamentals of Aerodynamics*, McGraw-Hill Companies, Inc., 3rd ed., 2001.

[21] Kuethe, A. M. and Chow, C.-Y., *Foundations of Aerodynamics: Bases of Aerodynamic Design*, John Wiley and Sons, Inc., 5th ed., 1997.

[22] Munk, M. M., "The Minimum Induced Drag of Aerofoils," NACA Rep. 121, 1921.

[23] Blackwell, J. A., "Numerical Method to Calculate the Induced Drag or Optimum Loading for Arbitrary Non-Planar Aircraft," NASA SP 405, May 1976.

[24] Drela, M. and Youngren, H., *AVL: User's Guide*, MIT, 77 Massachusetts Avenue, 33-207, Cambridge, MA 02139, http://web.mit.edu/drela/Public/web/avl.

[25] Drela, M., "XFOIL: An Analysis and Design System for Low Reynolds Number Airfoils," *Low Reynolds Number Aerodynamics*, edited by T. J. Mueller, Vol. 54 of *Lecture Notes in Engineering*, Springer-Verlag, New York, June 1989, pp. 1–12.